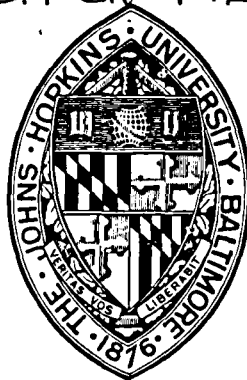


NASA-CR-172377

CMR-NASA-1

DRA



NASA-CR-172377  
19850018650

PROGRESS REPORT

MICROSTRUCTURE AND PROPERTIES OF RAPIDLY SOLIDIFIED ALLOYS

D. SHECHTMAN AND E. HOROWITZ

CENTER FOR MATERIALS RESEARCH  
THE JOHNS HOPKINS UNIVERSITY  
G. W. C. WHITING SCHOOL OF ENGINEERING  
BALTIMORE, MARYLAND 21218

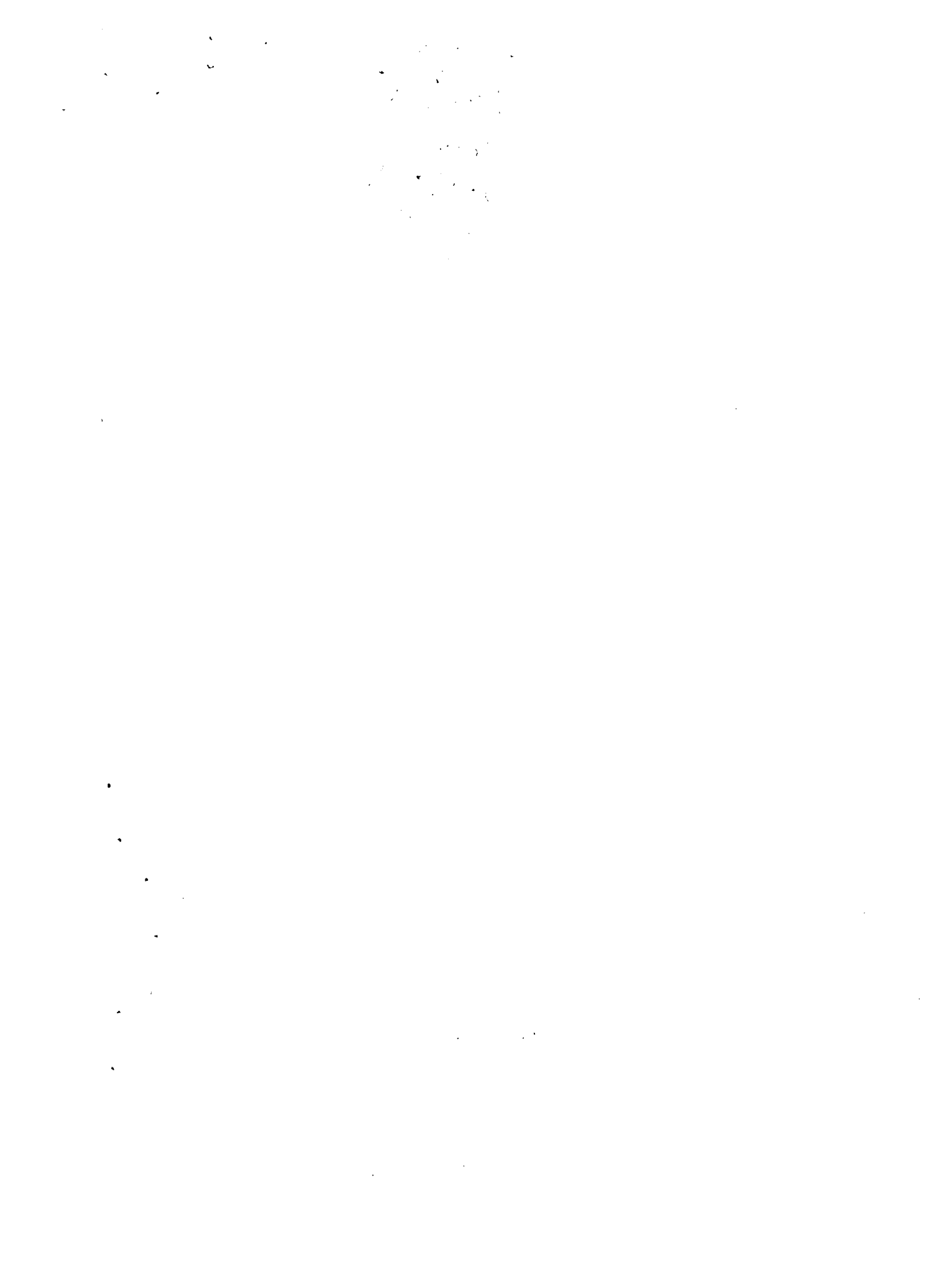
LIBRARY COPY

AUG 5 1985

LANGLEY RESEARCH CENTER  
LIBRARY, NASA  
HAMPTON, VIRGINIA

Sponsored by: National Aeronautics and Space Administration  
NASA Langley Research Center  
Hampton, Virginia 23665  
Grant Number: NAG 1-399

JANUARY 1984





**THE JOHNS HOPKINS UNIVERSITY**  
CENTER FOR MATERIALS RESEARCH  
MARYLAND HALL  
BALTIMORE, MARYLAND 21218

Emanuel Horowitz, Director

April 2, 1984

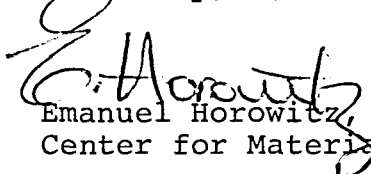
NASA Scientific and Technical  
Information Facility  
P. O. Box 8757  
Baltimore/Washington International Airport  
Maryland 21240

Dear Sir:

I am enclosing two copies of our report on "Microstructure and Properties of Rapidly Solidified Alloys" performed under NASA Grant No. 83-215. The microstructure of the aluminum alloys are discussed in this report and related to a unique set of micrographs which have been carefully reproduced in textbook quality so as to capture the details observed in the microscope.

Our next report will contain the results of our current experiments.

Sincerely,

  
Emanuel Horowitz, Director  
Center for Materials Research

EH:bjl  
Enclosures



TABLE OF CONTENTS

	<u>PAGE</u>
Executive Summary	vii
1. General	1
2. Optical Metallography and Scanning Electron Microscopy	1
3. Transmission Electron Microscopy	3
a) Al-1.6Fe-0.8Ce (No. 7) (Atomized in flue gas)	3
b) Al-4Cu-1Mg-1.5Fe-0.75Ce (No. 6) (Atomized in flue gas)	13
c) Al-3Li-1.5Cu-1Mg-0.5Co-0.2Zr (No. 2) (Vacuum atomized powder)	17
d) Al-3Li-1.5Cu-1Mg-0.5Co-0.2Zr (No. 3) (Ultrasonically atomized powder - Argon)	17
e) Al-3Li-1.5Cu-1Mg-0.5Co-0.2Zr (No. 4) (Ultrasonically atomized powder - Helium)	20
f) Al-4.4Cu-1.5Mg-1Fe-1Ni-0.2Zr (No. 5) (Vacuum atomized powder)	20
4. Elemental Distribution in the Cellular Structure	25
5. Summary	29



## LIST OF FIGURES

	<u>PAGE</u>
FIGURE 1. The alloy powder Al-1.6Fe-0.8Ce. Optical metallography x 400. (Sample No. 7).	2
FIGURE 2. The alloy powder Al-4Cu-1Mg-1.5Fe-0.75Ce. Optical metallography x 400. (Sample No. 6).	2
FIGURE 3. The alloy flakes Al-3Li-1.5Cu-1Mg-0.5Co-0.2Zr. Roller quenched, optical metallography x 400. (Sample No. 1).	2
FIGURE 4. The alloy powder Al-3Li-1.5Cu-1Mg-0.5Co-0.2Zr. Vacuum atomized, optical metallography x 400. (Sample No. 2).	2
FIGURE 5. The alloy powder Al-3Li-1.5Cu-1Mg-0.5Co-0.2Zr. Ultrasonically atomized in argon, optical metallography x 400. (Sample No. 3).	3
FIGURE 6. The alloy powder Al-3Li-1.5Cu-1Mg-0.5Co-0.2Zr. Ultrasonically atomized in helium, optical metallography x 400. (Sample No. 4).	3
FIGURE 7. The alloy powder Al-4.4Cu-1.5Mg-1Fe-1Ni-0.2Zr. Vacuum atomized, optical metallography x 400. (Sample No. 5).	3
FIGURE 8. The alloy powder Al-1.6Fe-0.8Ce. SEM. (Sample No. 7).	5
FIGURE 9. The alloy powder Al-4Cu-1Mg-1.5Fe-0.75Ce. SEM. (Sample No. 6).	5
FIGURE 10. The alloy flakes Al-3Li-1.5Cu-1Mg-0.5Co-0.2Zr. Roller quenched, SEM. (Sample No. 1).	6
FIGURE 11. The alloy powder Al-3Li-1.5Cu-1Mg-0.5Co-0.2Zr. Vacuum atomized, SEM. (Sample No. 2).	6
FIGURE 12. The alloy powder Al-3Li-1.5Cu-1Mg-0.5Co-0.2Zr. Ultrasonically atomized in argon, SEM. (Sample No. 3).	7
FIGURE 13. The alloy powder Al-3Li-1.5Cu-1Mg-0.5Co-0.2Zr. Ultrasonically atomized in helium, SEM. (Sample No. 4).	7



## LIST OF FIGURES

	<u>PAGE</u>
FIGURE 14. The alloy powder Al-4.4Cu-1.5Mg-1Fe-1Ni-0.2Zr. Vacuum atomized, SEM. (Sample No. 5).	8
FIGURE 15. Al-1.6Fe-0.8Ce. Small cells are formed at high velocity of solidification. (Sample No. 7).	9
FIGURE 16. Al-1.6Fe-0.8Ce. Large cells are formed at low velocity of solidification (Sample No. 7).	9
FIGURE 17. Al-1.6Fe-0.8Ce. The microstructure of a powder particle as a function of distance from the nucleation spot. Dashed line marks transition from adiabatic to non-adiabatic solidification region. (Sample No. 7).	11
FIGURE 18. Al-1.6Fe-0.8Ce. Illustrated on two nucleation sites in one particle. Two adiabatic zones are observed and the rest of the particle consists of cells. (Sample No. 7).	14
FIGURE 19. Al-4Cu-1Mg-1.5Fe-0.75Ce. Cell formation with marked cell boundaries and strained cell interiors. (Sample No. 6).	14
FIGURE 20. Al-4Cu-1Mg-1.5Fe-0.75Ce. High density of dislocations in the cell interior. (Sample No. 6).	15
FIGURE 21. Al-4Cu-1Mg-1.5Fe-0.75Ce. Rings indicating a microcrystalline or amorphous phase at the cell boundaries. (Sample No. 6).	15
FIGURE 22. Al-4Cu-1Mg-1.5Fe-0.75Ce. Dark field image from ring in Figure 21. Cell boundaries are clearly marked. (Sample No. 6).	16
FIGURE 23. Al-4Cu-1Mg-1.5Fe-0.75Ce. Nucleation center at the interior of the particle. Such centers originate in a small spherulite that solidifies first. (Sample No. 6).	16
FIGURE 24. Al-3Li-1.5Cu-1Mg-0.5Co-0.2Zr. Vacuum atomized. Large cells and feathery phase at the cell boundary. (Sample No. 2).	18



## LIST OF FIGURES

	<u>PAGE</u>
FIGURE 25. Al-3Li-1.5Cu-1Mg-0.5Co-0.2Zr. Vacuum atomized. Feathery phase at all boundaries. (Sample No. 2).	18
FIGURE 26. Al-3Li-1.5Cu-1Mg-0.5Co-0.2Zr. Ultrasonic atomization in argon. The cellular microstructure contains a phase at the cell boundary and dislocations within the cells. (Sample No. 3).	19
FIGURE 27. Al-3Li-1.5Cu-1Mg-0.5Co-0.2Zr. Ultrasonic atomization in argon. A continuous phase at the cell boundary. (Sample No. 3).	19
FIGURE 28. Al-3Li-1.5Cu-1Mg-0.5Co-0.2Zr. Ultrasonic atomization in argon. Fine precipitates within the cells. (Sample No. 3).	21
FIGURE 29. Al-3Li-1.5Cu-1Mg-0.5Co-0.2Zr. Ultrasonic atomization in argon. Selected area diffraction pattern indicates extra spots at half distance of the (002) reflection originated from fine particles in Figure 28. (Sample No. 3).	21
FIGURE 30. Al-3Li-1.5Cu-1Mg-0.5Co-0.2Zr. Ultrasonic atomization in helium. A cellular microstructure. Cell size is up to 2 $\mu$ m and the cells are heavily strained. (Sample No. 4).	22
FIGURE 31. Al-3Li-1.5Cu-1Mg-0.5Co-0.2Zr. Ultrasonic atomization in helium. Particles at cell boundaries. (Sample No. 4).	22
FIGURE 32. Al-3Li-1.5Cu-1Mg-0.5Co-0.2Zr. Ultrasonic atomization in helium. High density of dislocation within the cells, weak beam dark field. (Sample No. 4).	23
FIGURE 33. Al-3Li-1.5Cu-1Mg-0.5Co-0.2Zr. Ultrasonic atomization in helium. High density of particles in some of the cells. (Sample No. 4).	23
FIGURE 34. Al-3Li-1.5Cu-1Mg-0.5Co-0.2Zr. Ultrasonic atomization in helium. Selected area diffraction pattern of particles in Figure 33. (Sample No. 4).	24



LIST OF FIGURES

	<u>PAGE</u>
FIGURE 35. Al-4.4Cu-1.5Mg-1Fe-1Ni-0.2Zr. Vacuum atomized powder. Large cells, measuring up to 5 $\mu$ m in length are formed. (Sample No. 5).	24
FIGURE 36. Al-4.4Cu-1.5Mg-1Fe-1Ni-0.2Zr. Vacuum atomized powder. Particles are formed at the cell boundary. (Sample No. 5).	26
FIGURE 37. Al-4.4Cu-1.5Mg-1Fe-1Ni-0.2Zr. Vacuum atomized powder. The cell interior contains a high density of dislocations. (Sample No. 5).	26



LIST OF TABLES

	<u>PAGE</u>
TABLE A. Compositional analysis of cell interior and cell boundary for the alloy Al-4Cu-1Mg-1.5Fe-0.75Ce (Sample No. 6)	27
TABLE B. Compositional analysis of cell interior and cell boundary for the alloy Al-4.4Cu-1.5Mg-1Fe-1Ni-0.2Zr (Sample No. 5)	28
TABLE C. Equilibrium partition coefficients for solidification of primary aluminum phase	29



## EXECUTIVE SUMMARY

This progress report describes the research performed by The Johns Hopkins University Center for Materials Research on the microstructure and properties of rapidly solidified aluminum alloys under NASA Grant NAG-1-399 in support of the program of the Metals and Ceramics Group at the NASA Langley Research Center. The seven aluminum alloys in the form of thin foils were studied by a variety of techniques including optical metallography, scanning electron microscopy (SEM), and transmission electron microscopy (TEM). The microstructure of six of the samples (No. 2,3,4,5,6,7) were evaluated using a Philips 400 STEM and a JEOL 120CX STEM and details of the microstructural characteristics are presented along with a discussion of the solidification process. For example, Sample No. 6, Al-4Cu-1Mg-1.5Fe-0.75Ce, was found to be cellular in structure with cell sizes measuring up to 1 $\mu$ m and with cells containing a high density of dislocations. Information on the nature of the cell boundaries in the alloys is also provided. Data on the compositional analysis in the cell and the cell boundary is given for two alloys.

The work thus far has provided a better understanding of the microstructure of the rapidly solidified aluminum alloys prepared by a variety of techniques such as roller quenching, the vacuum atomized procedure, ultrasonically atomized in inert atmospheres, and atomized in flue gas.



## 1. General

Seven samples of aluminum alloy powder were obtained from MCDONNELL DOUGLAS ASTRONAUTICS COMPANY in St. Louis, Missouri. The powders were made under NASA contract entitled "Consolidation Processing Parameters and Alternative Processing Methods for Powder Metallurgy Al-Cu-Mg-x-x Alloys" (Contract No. NASA 1-16967). The nominal compositions of the powders are:

- (1) Al-3 Li-1.5 Cu-1 Mg-0.5 Co-0.2 Zr (Roller quenched flakes-chopped)
- (2) Al-3 Li-1.5 Cu-1 Mg-0.5 Co-0.2 Zr (Vacuum atomized powder)
- (3) Al-3 Li-1.5 Cu-1 Mg-0.5 Co-0.2 Zr (Ultrasonically atomized powder-Argon)
- (4) Al-3 Li-1.5 Cu-1 Mg-0.5 Co-0.2 Zr (Ultrasonically atomized powder-Helium)
- (5) Al-4.4 Cu-1.5 Mg-1 Fe-1 Ni-0.2 Zr (Vacuum atomized powder)
- (6) Al-4 Cu-1 Mg-1.5 Fe-0.75 Ce\* (Atomized in flue gas)
- (7) Al-1.6 Fe-0.8 Ce (Atomized in flue gas)

## 2. Optical Metallography and Scanning Electron Microscopy

The powders were cold mounted and prepared for metallographic examination in the optical microscope, and the results are given in Figures 1-7. All the micrographs are presented in a standard magnification of x400. A characteristic cellular structure is observed in all the powders, and a more detailed description of the structure will be given later

\*On analysis the sample was found to have the following composition: Al-3.8Cu-1Mg-1.3Fe-0.7Ce.



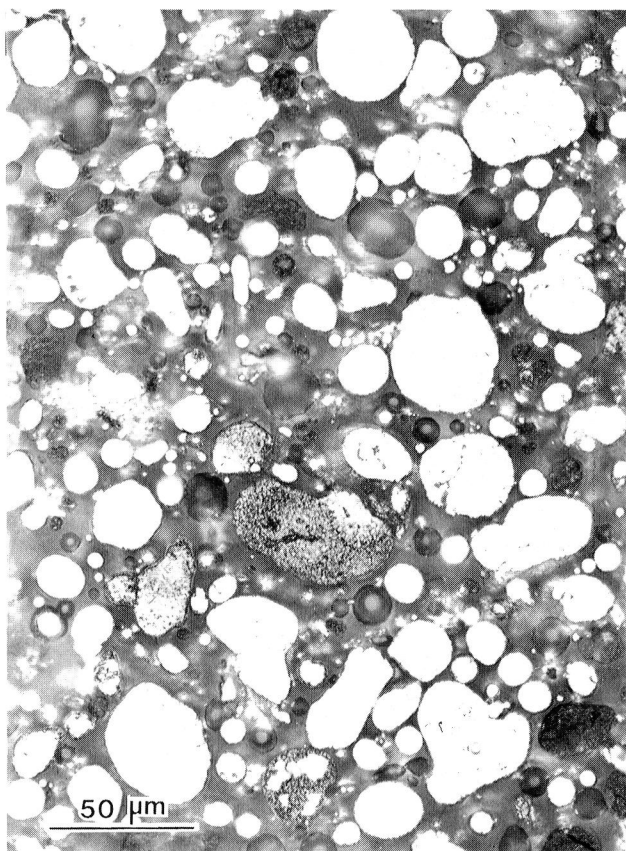


FIGURE 1.  
The alloy powder Al-1.6Fe-0.8Ce. Optical metallography x 400.  
(Sample No. 7).

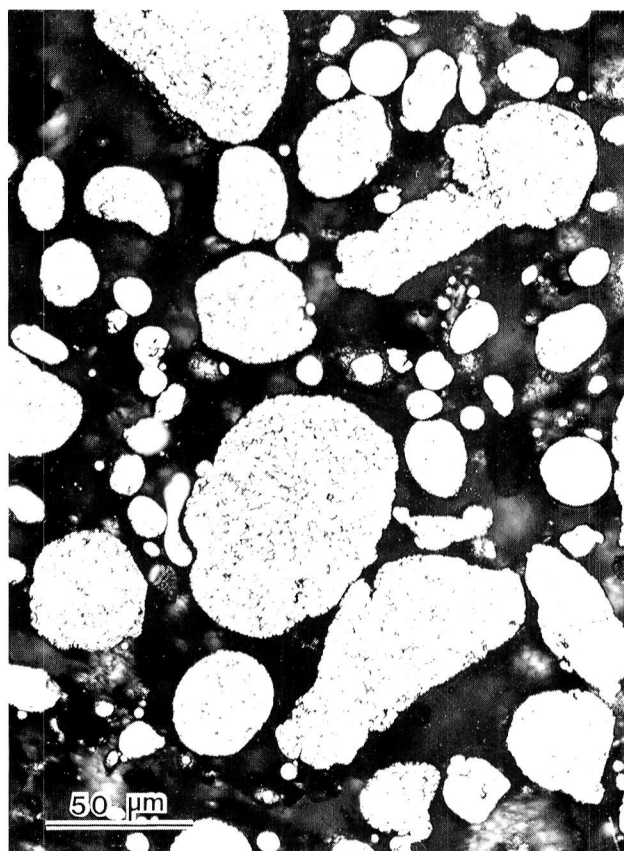


FIGURE 2.  
The alloy powder Al-4Cu-1Mg-1.5Fe-0.75Ce. Optical metallography x 400.  
(Sample No. 6).

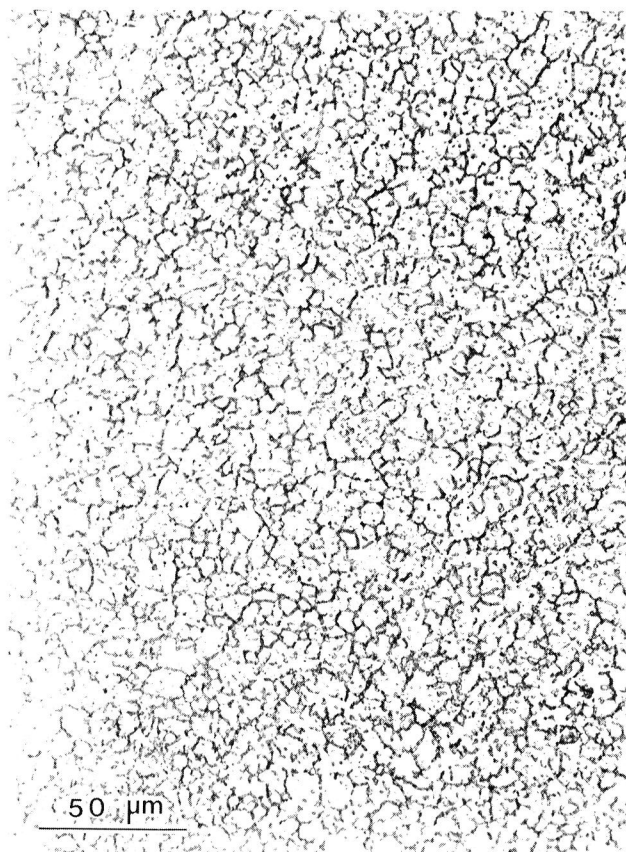


FIGURE 3.  
The alloy flakes Al-3Li-1.5Cu-1Mg-0.5Co-0.2Zr. Roller quenched,  
optical metallography x 400. (Sample No. 1).

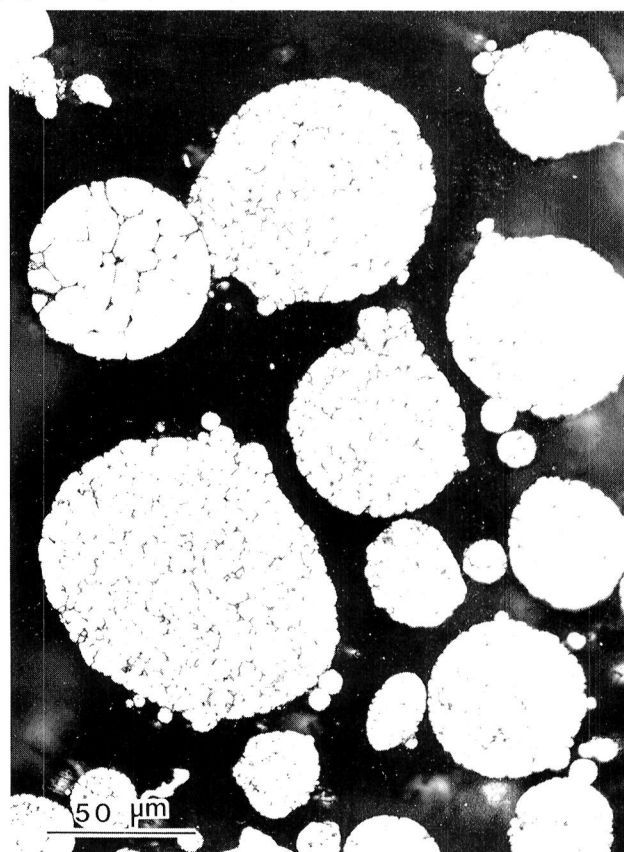


FIGURE 4.  
The alloy powder Al-3Li-1.5Cu-1Mg-0.5Co-0.2Zr. Vacuum atomized,  
optical metallography x 400. (Sample No. 2).



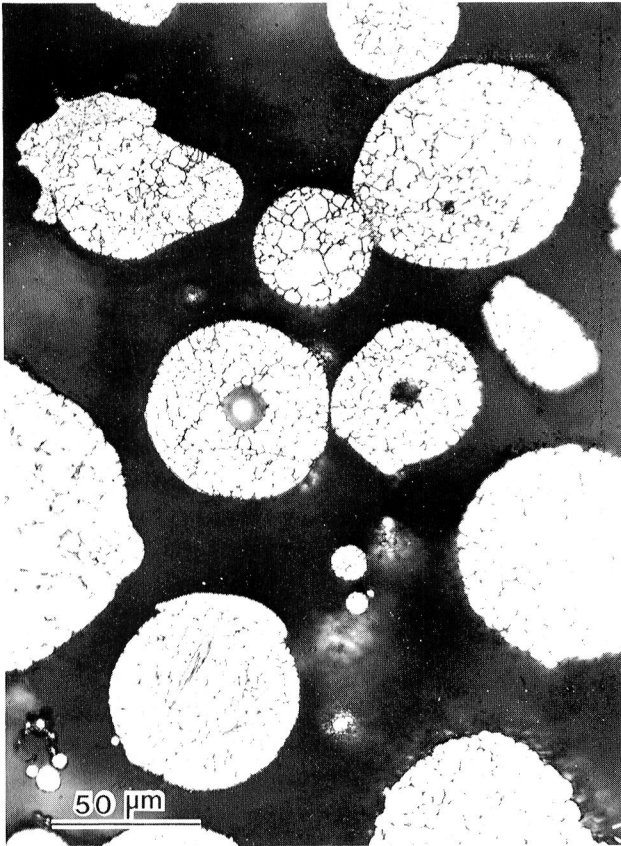


FIGURE 5.  
The alloy powder Al-3Li-1.5Cu-1Mg-0.5Co-0.2Zr. Ultrasonically atomized in argon, optical metallography x 400. (Sample No. 3).

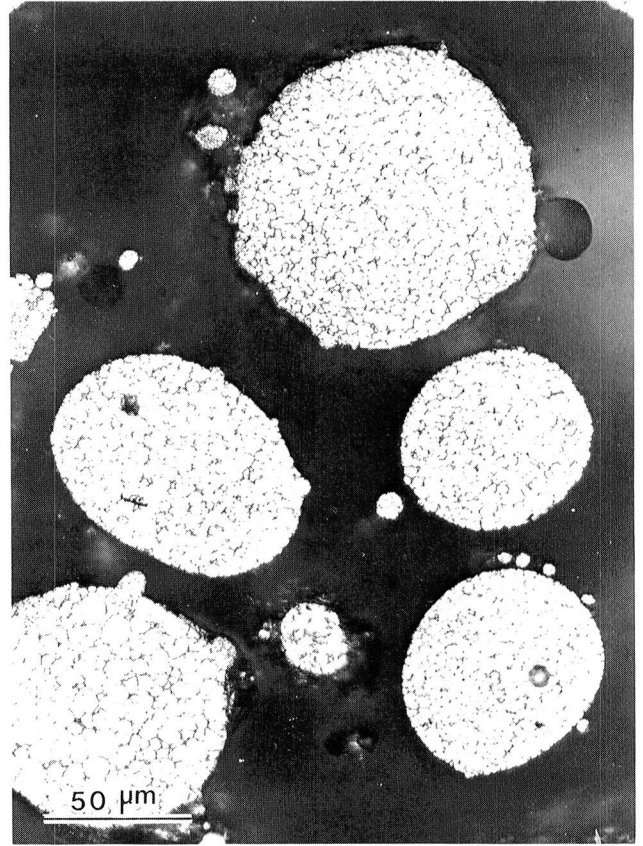


FIGURE 6.  
The alloy powder Al-3Li-1.5Cu-1Mg-0.5Co-0.2Zr. Ultrasonically atomized in helium, optical metallography x 400. (Sample No. 4).

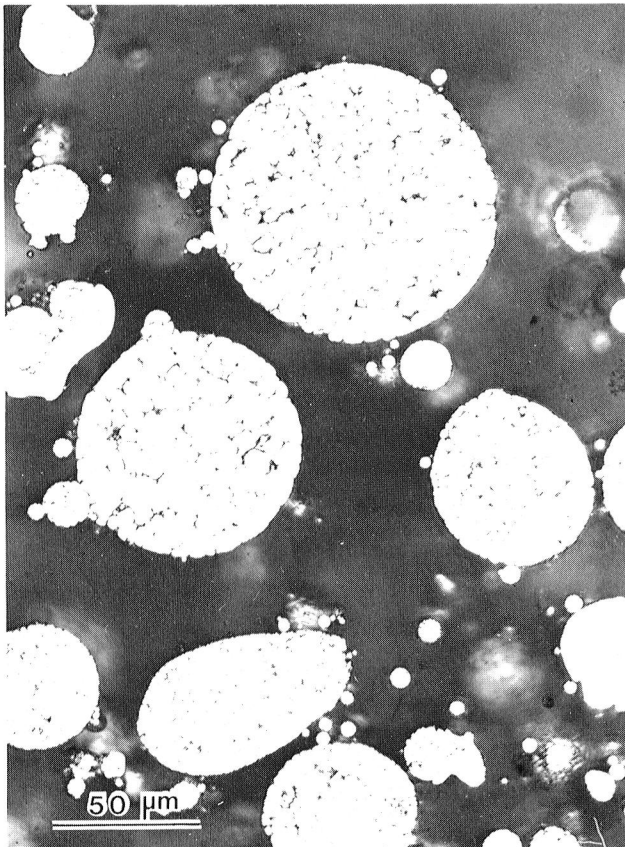


FIGURE 7.  
The alloy powder Al-4.4Cu-1.5Mg-1Fe-1Ni-0.2Zr. Vacuum atomized, optical metallography x 400. (Sample No. 5).



in this report. The roller quenched flakes (R. Q. #1) are distinctively different in shape than the other alloys and the technique used in their formation resembles in principle the melt spinning technique (except for the fact that in the melt spinning process the heat flow is principally unidirectional). The shape of the various powders (No. 1-7) is shown in the SEM micrographs, Figs. 8-14. The powders (except the flakes) are round but not spherical and all of them show a large range of size distribution.

### 3. Transmission Electron Microscopy

Thin foils of the powders were prepared by cold compaction of the powders to a disc shape which was followed by standard electropolishing. The foils thus obtained have large regions of electron transparent materials which cover many powder particles. The powders were studied in a Philips 400 STEM and in a JEOL 120CX STEM. The results obtained for the microstructure of the powders in their as received condition will be given here.

#### a. Al-1.6 Fe 0.8 Ce (No. 7)

The microstructure of the alloy as observed by transmission electron microscopy is cellular with cell sizes varying between  $0.1\mu\text{m}$  to  $1\mu\text{m}$  (Fig. 15 and 16) with a large proportion of the cells closer to the smaller size. Since the cell size is a direct function of the solidification rate, and its length indicates the direction of the solidifying front,



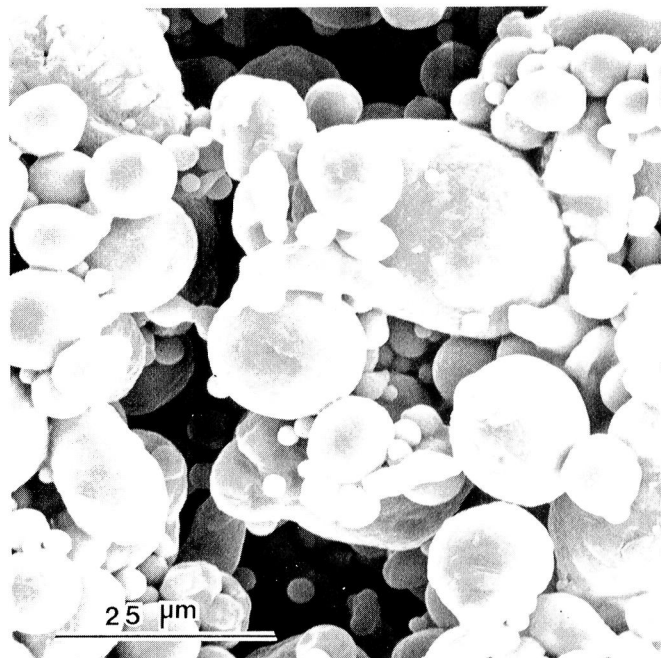
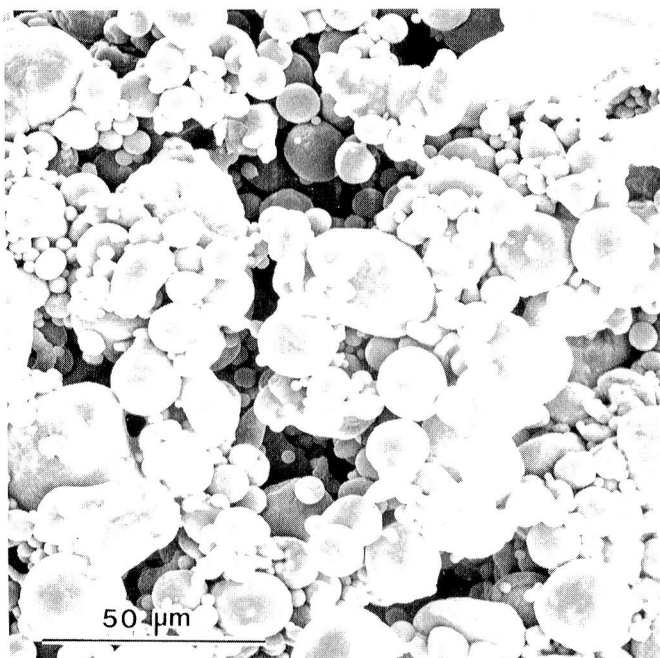


FIGURE 8.  
The alloy powder Al-1.6Fe-0.8Ce. SEM. (Sample No. 7).

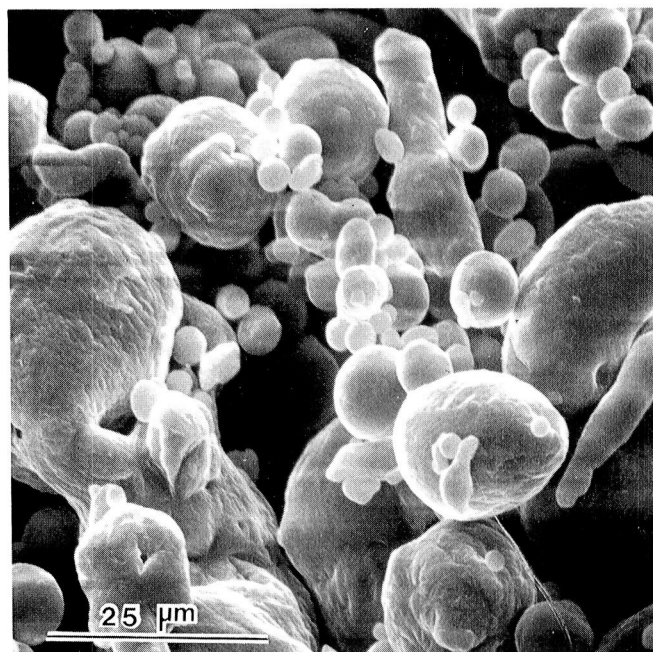
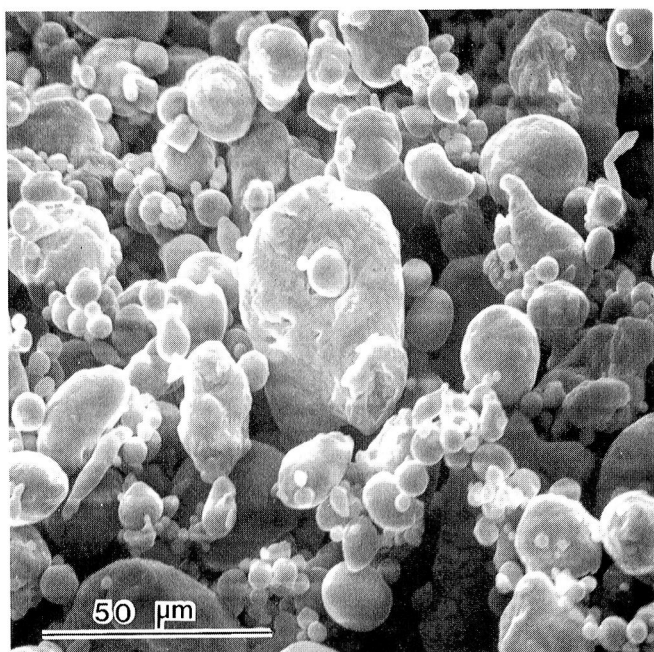


FIGURE 9.  
The alloy powder Al-4Cu-1Mg-1.5Fe-0.75Ce. SEM. (Sample No. 6).



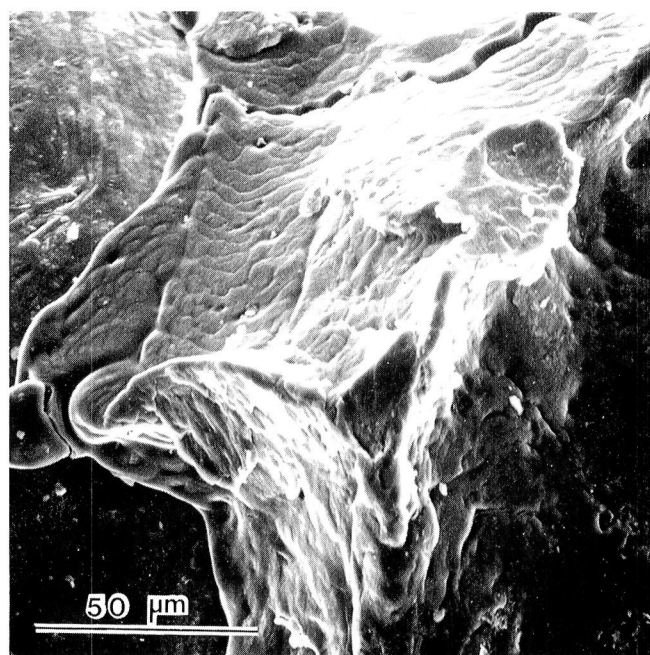
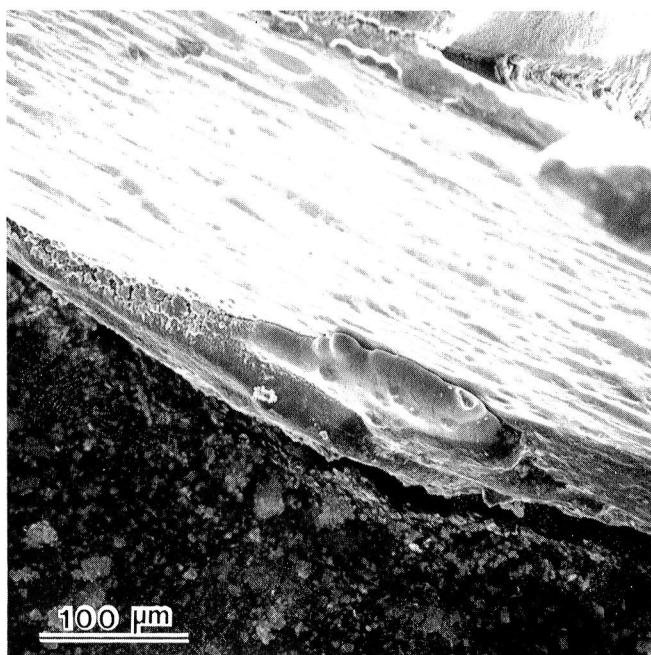


FIGURE 10.  
The alloy flakes Al-3Li-1.5Cu-1Mg-0.5Co-0.2Zr. Roller quenched, SEM. (Sample No. 1).

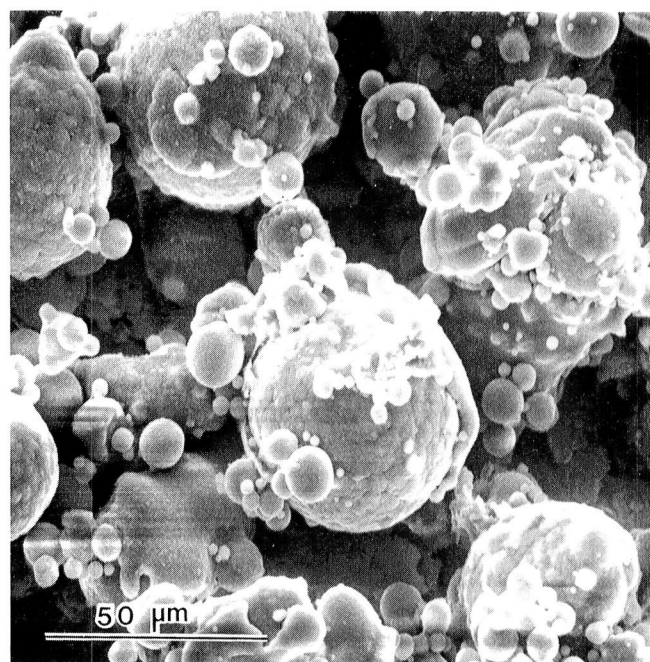
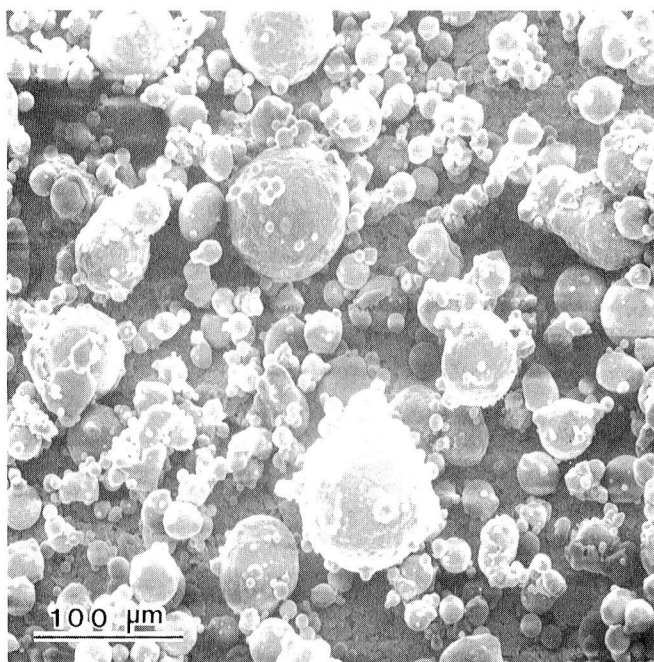


FIGURE 11.  
The alloy powder Al-3Li-1.5Cu-1Mg-0.5Co-0.2Zr. Vacuum atomized, SEM. (Sample No. 2).



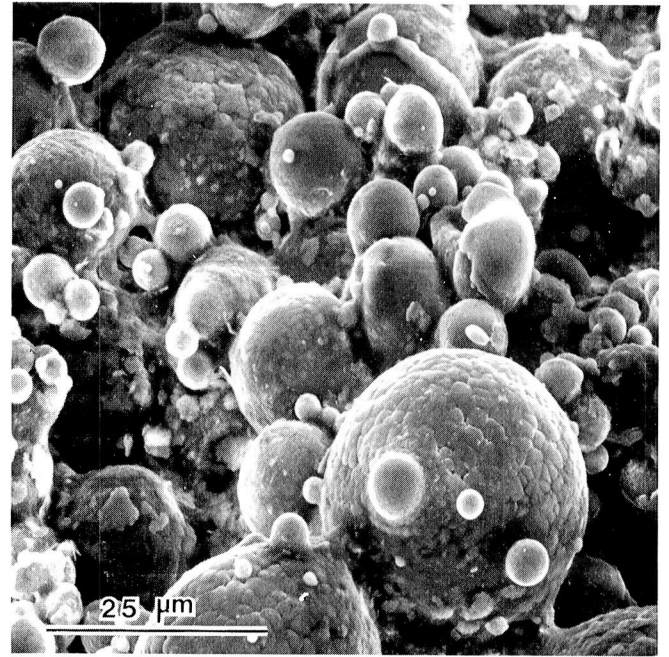
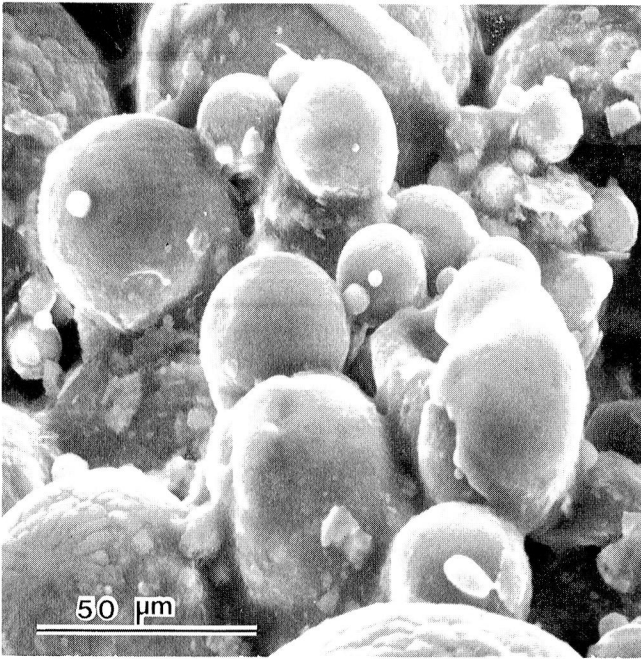


FIGURE 12.  
The alloy powder Al-3Li-1.5Cu-1Mg-0.5Co-0.2Zr. Ultrasonically atomized in argon, SEM. (Sample No. 3).

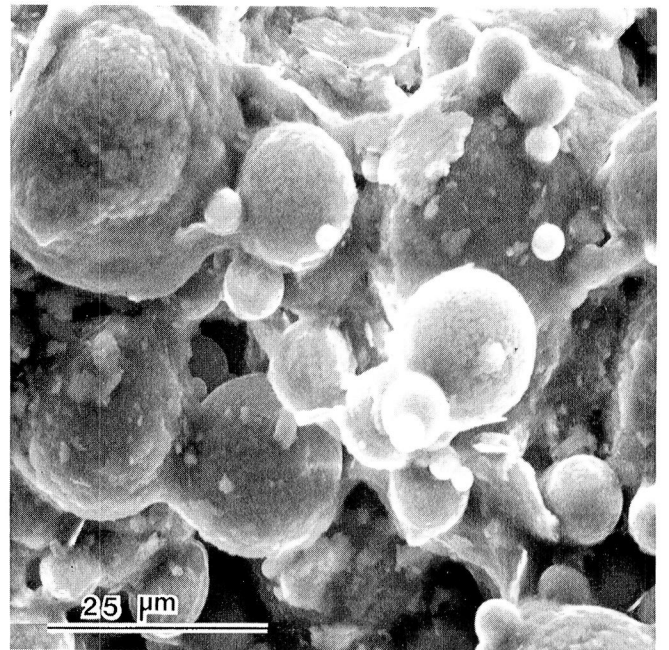
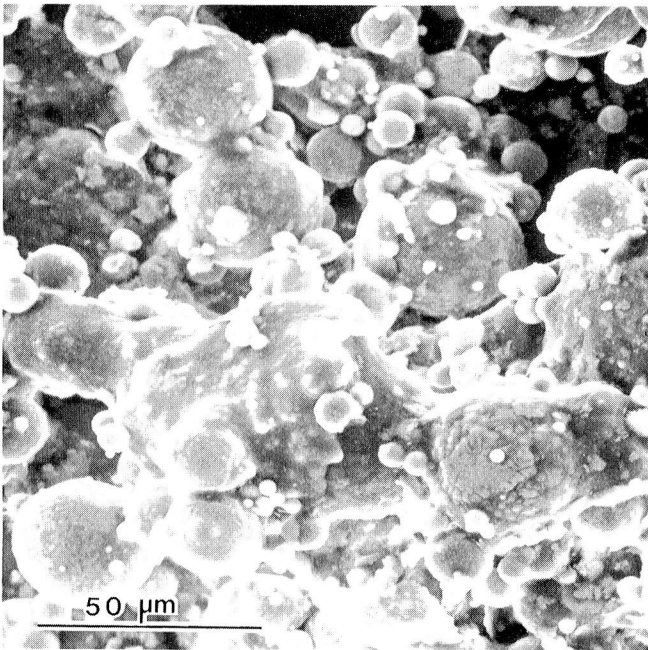


FIGURE 13.  
The alloy powder Al-3Li-1.5Cu-1Mg-0.5Co-0.2Zr. Ultrasonically atomized in helium, SEM. (Sample No. 4).



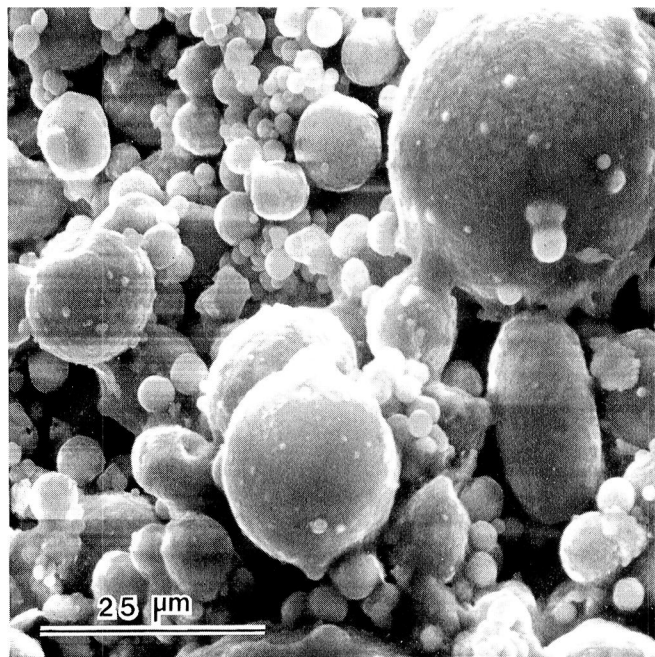
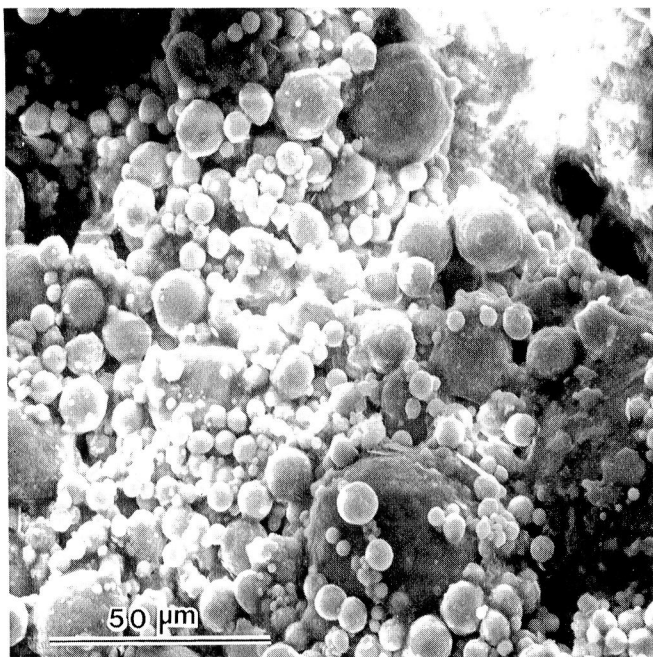


FIGURE 14.  
The alloy powder Al-4.4Cu-1.5Mg-1Fe-1Ni-0.2Zr. Vacuum atomized, SEM. (Sample No. 5).



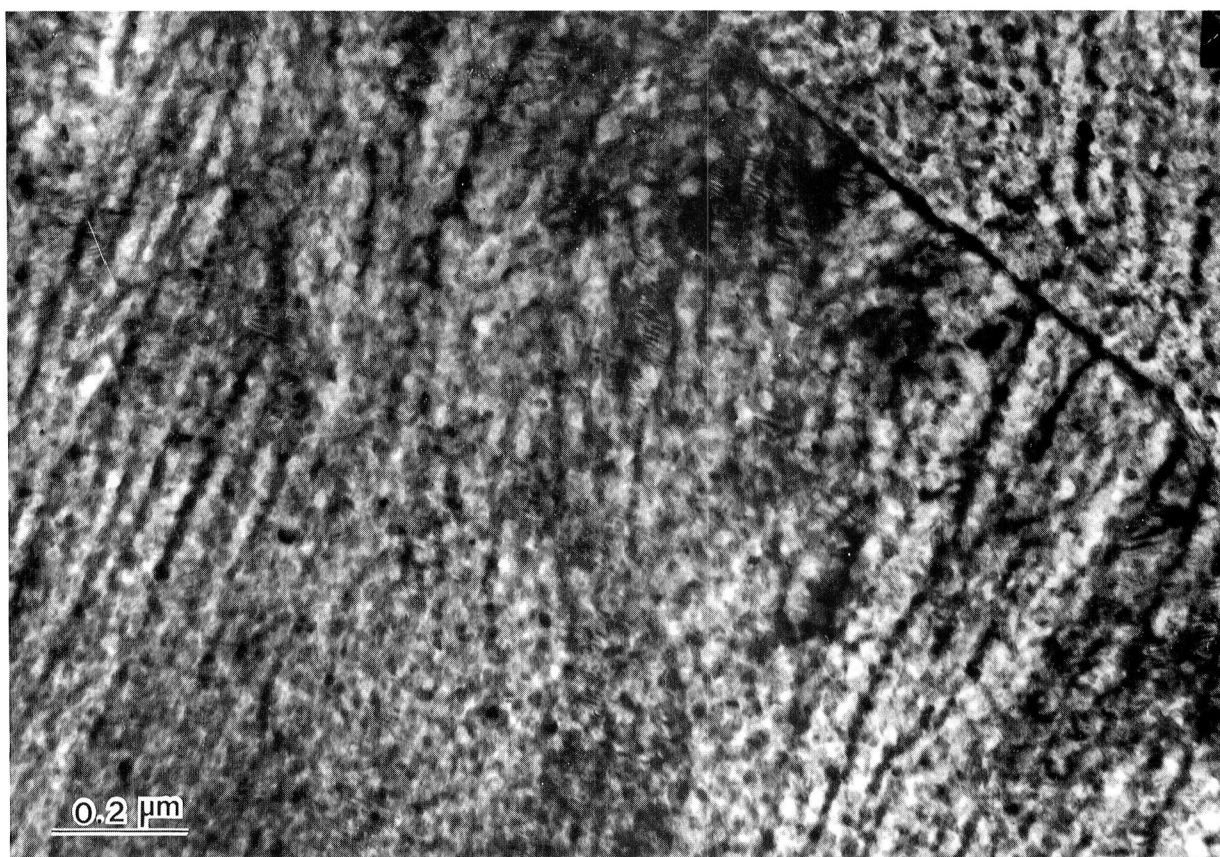


FIGURE 15.  
Al-1.6Fe-0.8Ce. Small cells are formed at high velocity of solidification. (Sample No. 7).

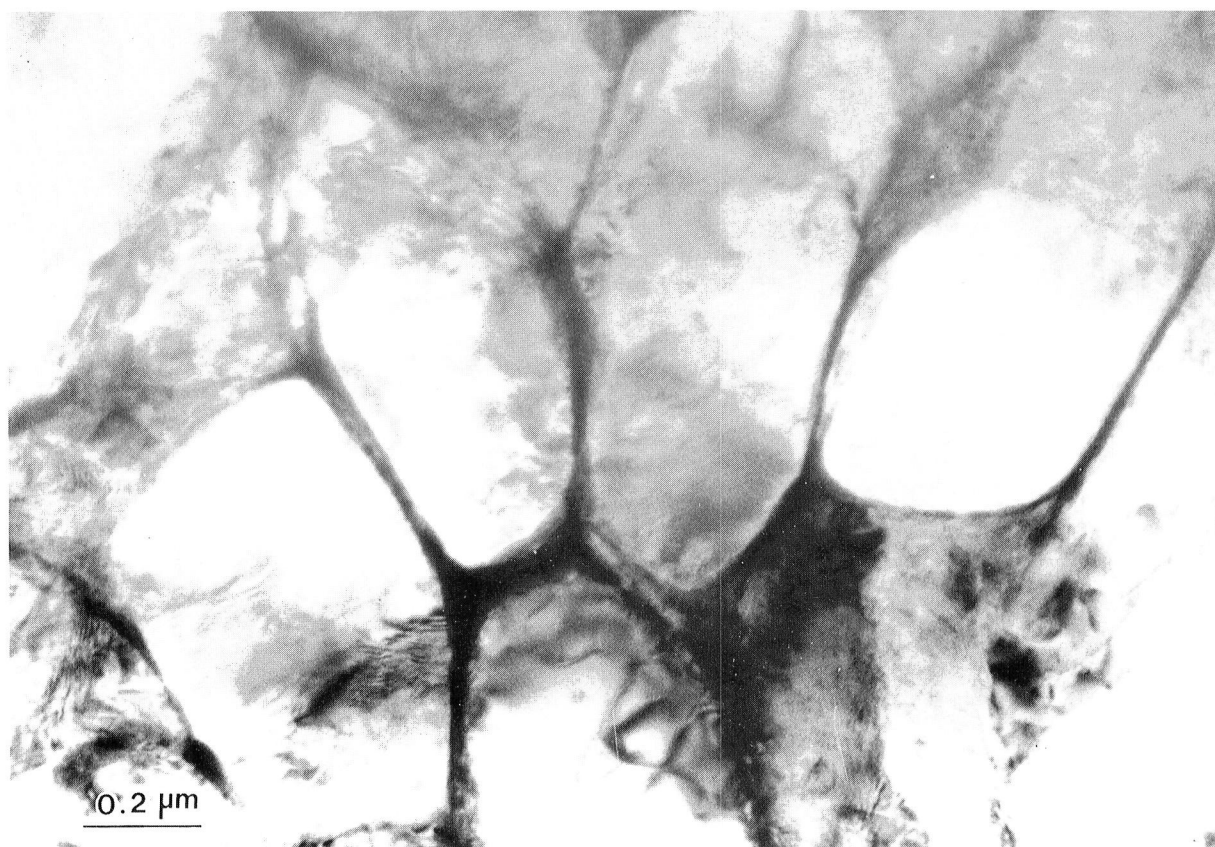


FIGURE 16.  
Al-1.6Fe-0.8Ce. Large cells are formed at low velocity of solidification (Sample No. 7).



conclusions can be drawn as to the location of the first solid nucleus and the relative velocity of the solidification front. This can be illustrated on the composite Fig. 17. The micrograph is one of a particle whose size is equal or larger than  $5\mu\text{m}$ . The solidification of the particle starts at the point marked A on the surface of the particle. No cells are formed at the first solidification stage, and the particles which are observed result from a solid state transformation. When the solidification front reaches a certain distance from the starting position, an abrupt change occurs in the microstructure.

The position of the front when the change occurs is marked by a dashed line. From this position on, cells are formed and the growth of the cell size is rather moderate until solidification is completed. This behavior of the solidifying front is typical for aluminum alloy powders and its origin is in the heat extraction process in the solidifying front.

The following sequence of events is presumed to occur in the solidifying particle. Upon cooling a certain degree of bulk undercooling is achieved in the still liquid droplet. The degree of undercooling can be calculated from the shape of the front as will be shown later. Solidification starts in most cases on the outer surface of the droplet, but in some cases inner nucleation is observed. As the solidification front progresses, the heat of freezing is released and absorbed by the undercooled particle. This happens because of the preferred heat transfer in the alloy as compared to that into the



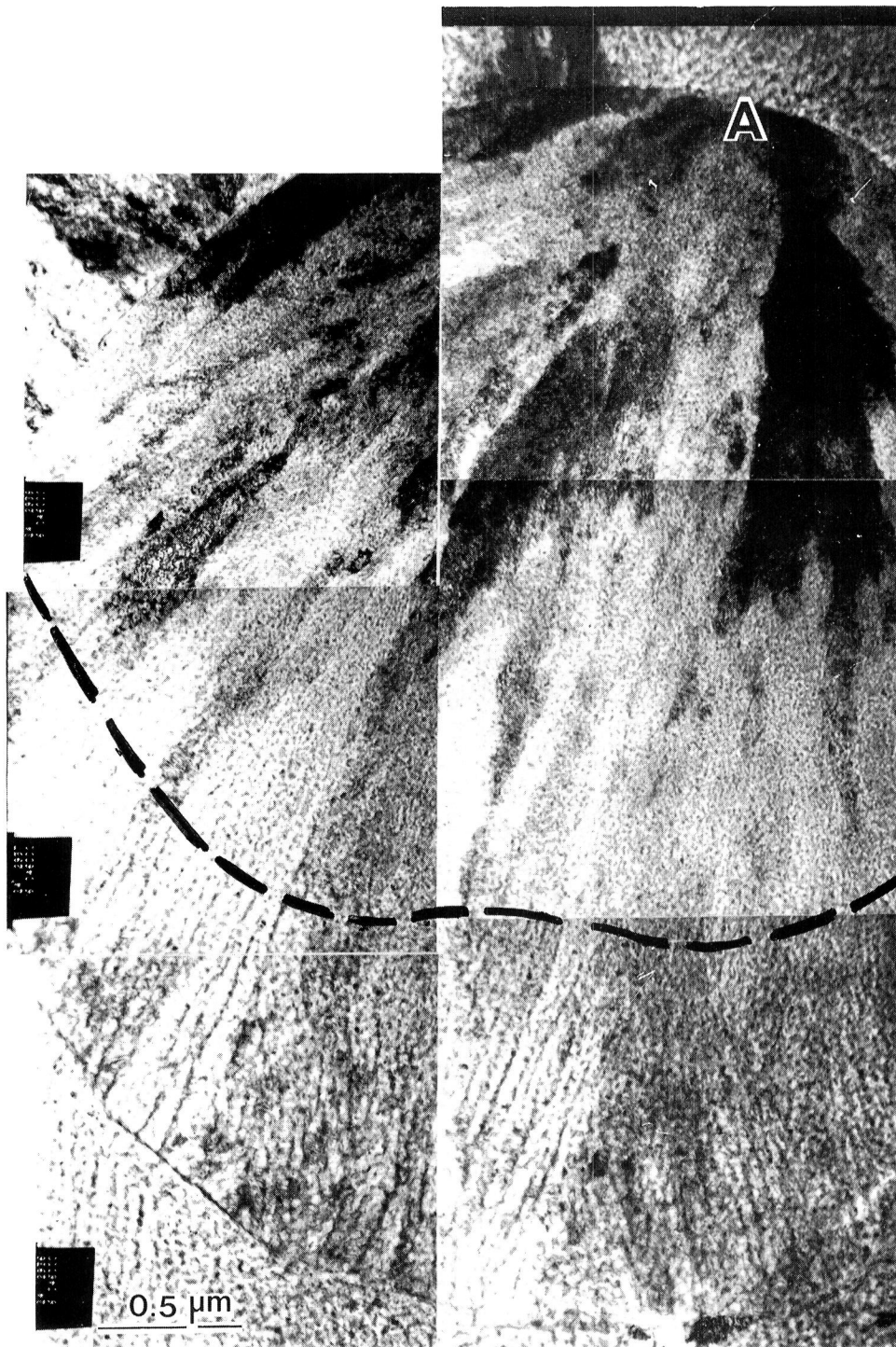


FIGURE 17.  
Al-1.6Fe-0.8Ce. The microstructure of a powder particle as a function of distance from the nucleation spot. Dashed line marks transition from adiabatic to non-adiabatic solidification region. (Sample No. 7).



environment. The high velocity of the solidifying front is impeded when the particle is reheated and is not able to absorb the heat of freezing. At this stage the heat transfer to the environment becomes the governing factor that controls the velocity of the solidifying front.

The velocity of the solidification front decreases at this stage and thus the cells start to form. The two solidification stages just described may be regarded as an adiabatic stage in which the main heat transfer is done within the particle and a nonadiabatic stage in which heat is transferred out of the particle. An example of the calculated undercooling will be done on the particle presented in Fig. 17. Heat balance done on the particle at the instant of the completion of the adiabatic stage yields the following:

$$1. \quad mL = MC\Delta T$$

Where:  $m$  is the mass of the adiabatically solidified volume

$L$  is the heat of freezing

$M$  is the mass of the particle

$C$  is the specific heat

$\Delta T$  is the amount of undercooling

$$2. \quad \Delta T = \frac{L}{C} \left(\frac{r}{R}\right)^3$$

for  $\left(\frac{r}{R}\right) = 0.7$  as is the case in this particle we obtain

$$\Delta T = 130^\circ\text{C}.$$

This high degree of bulk undercooling is below the  $T_0$  point of the alloy, and the beginning of the solidification process is

thus done at a temperature at which no segregation (cell formation) can occur. This supports the hypothesis that the particles observed in this region result from solid state transformation.

Some particles contain more than one nucleation site, as illustrated in Fig. 18. In such cases, several regions of adiabatic solidification are formed and these are surrounded by nonadiabatic-cellular structure.

b. Al-4 Cu-1 Mg-1.5 Fe-0.75 Ce (No. 6)

The microstructure of this alloy is cellular, with cell sizes measuring up to  $1\mu\text{m}$  (Fig. 19). The cells contain a high density of dislocations (Fig. 20) which is not characteristic of many cellular structures, but is rather common in the alloys examined in this study. This may indicate an internal stress developed at the early stages of precipitation.

The selected area diffraction pattern (Fig. 21) contains rings resulting from a microcrystalline or amorphous phase in the cell boundaries. A dark field image taken from the strongest ring is shown in Fig. 22 in which the cell boundary phase can be clearly observed. Although the solidification sequence in this alloy seems similar to that of the other powders examined in this study, there are occasions in which nucleation sites are found at the interior of the particle. Such is the case shown in Fig. 23. In this example the nucleation site is located at the center of the particle and the cells



FIGURE 18.  
Al-1.6Fe-0.8Ce. Illustrated on two nucleation sites in one particle. Two adiabatic zones are observed and the rest of the particle consists of cells. (Sample No. 7).

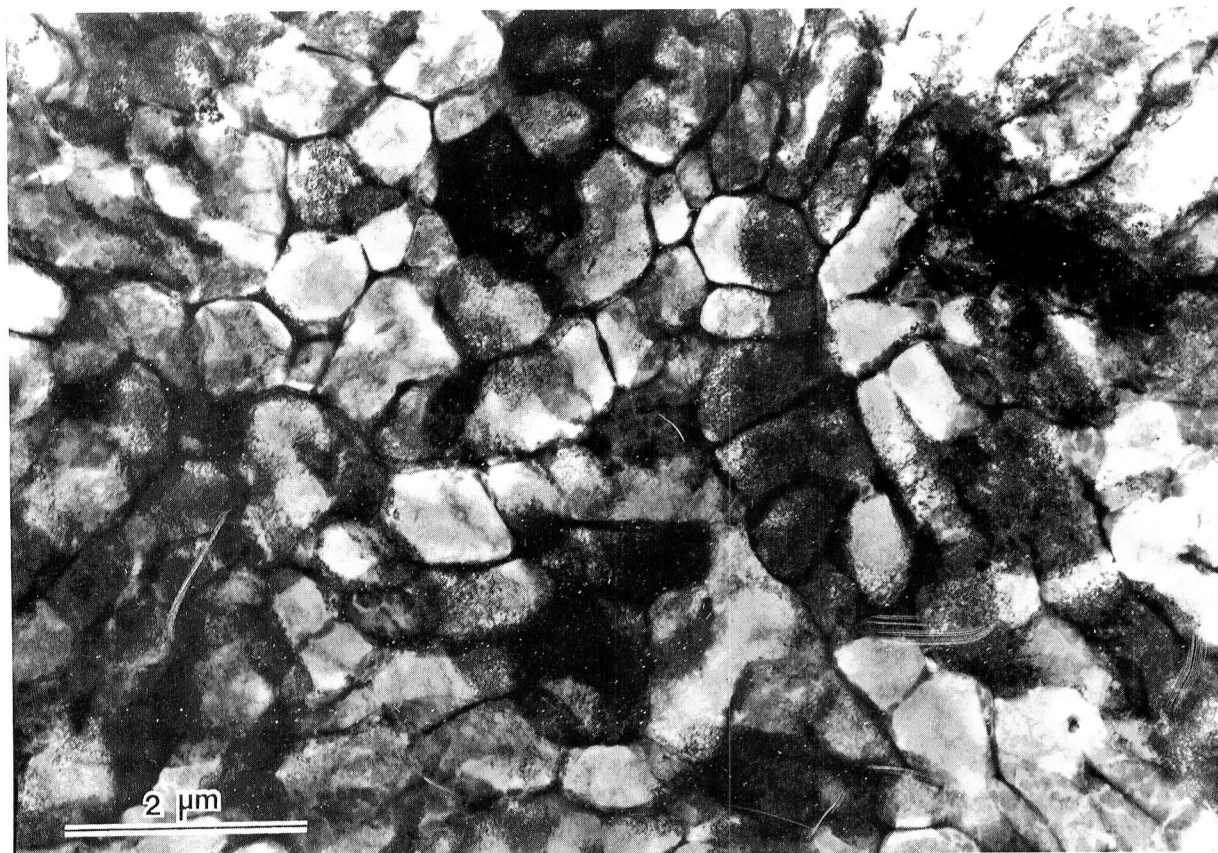


FIGURE 19.  
Al-4Cu-1Mg-1.5Fe-0.75Ce. Cell formation with marked cell boundaries and strained cell interiors. (Sample No. 6).



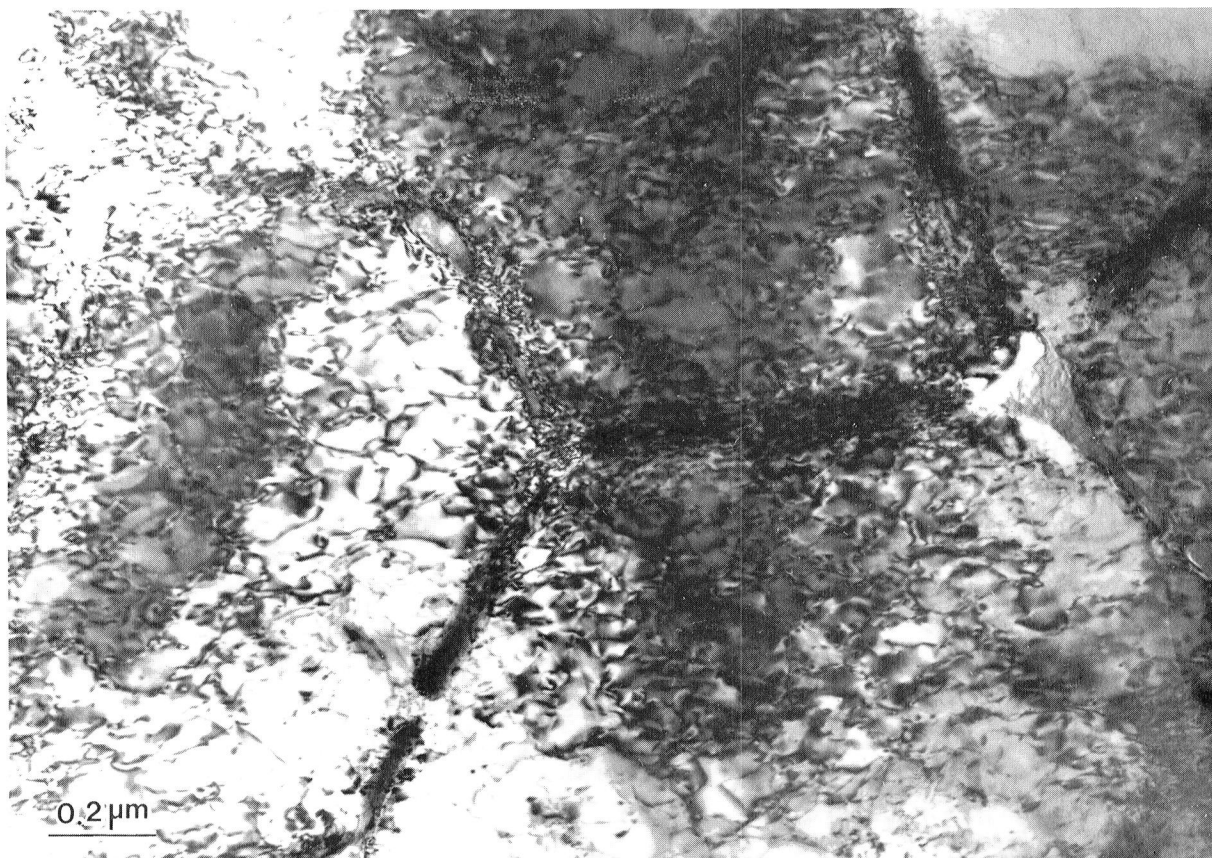


FIGURE 20.  
Al-4Cu-1Mg-1.5Fe-0.75Ce. High density of dislocations in the cell interior. (Sample No. 6).

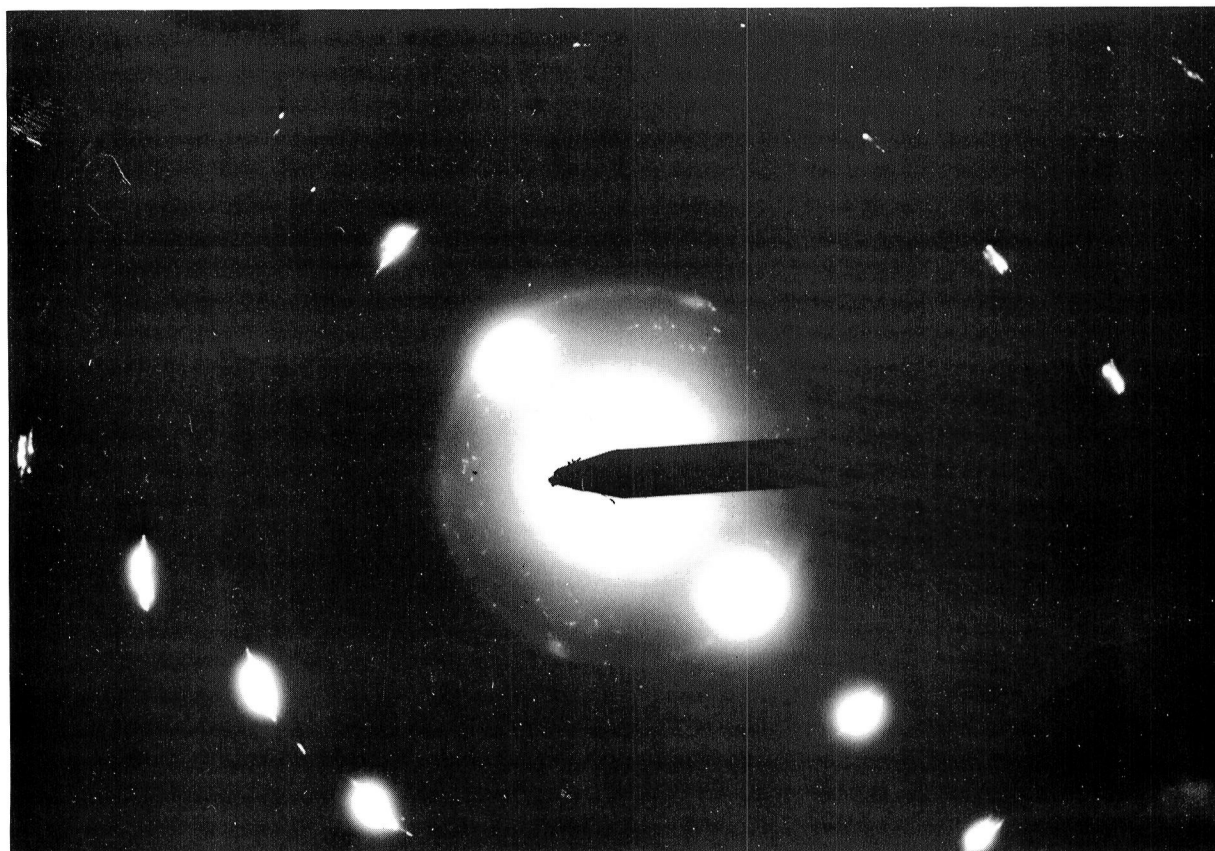


FIGURE 21.  
Al-4Cu-1Mg-1.5Fe-0.75Ce. Rings indicating a microcrystalline or amorphous phase at the cell boundaries. (Sample No. 6).



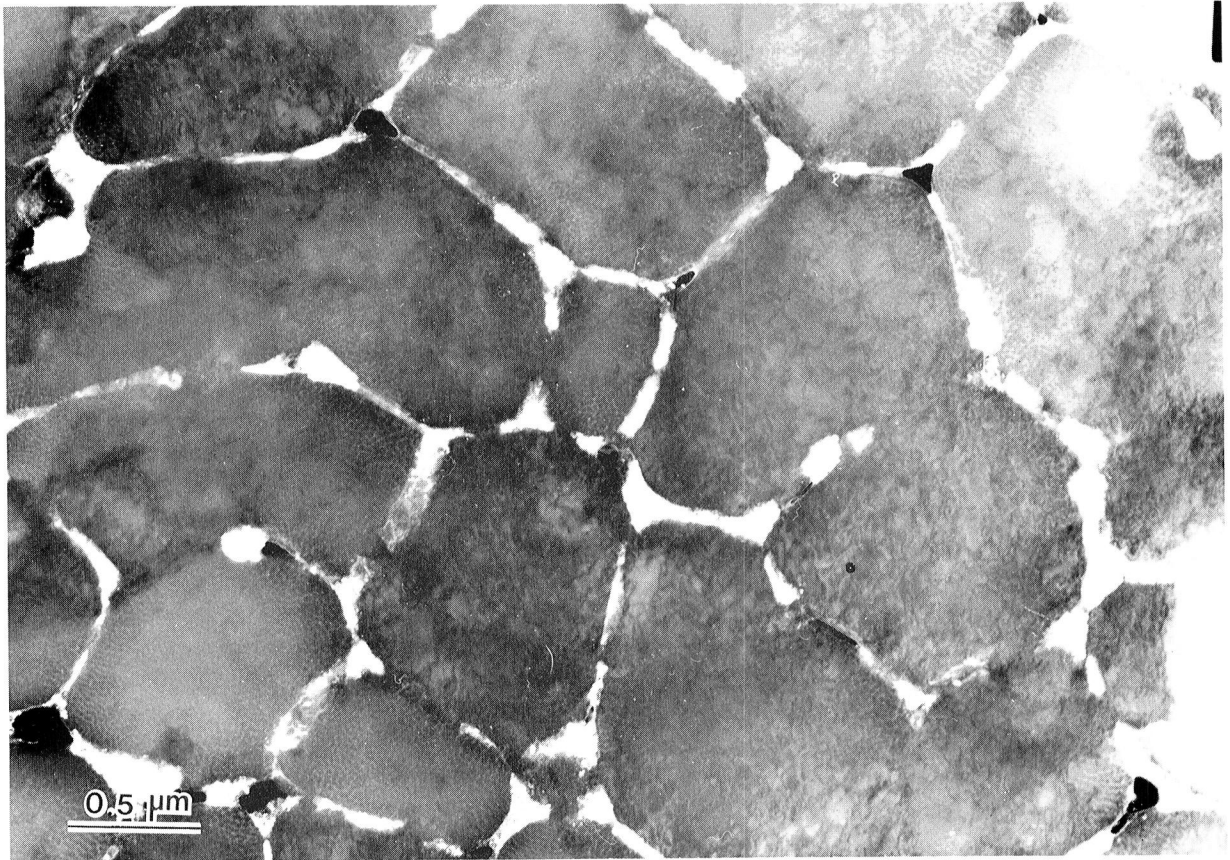


FIGURE 22.  
Al-4Cu-1Mg-1.5Fe-0.75Ce. Dark field image from ring in Figure 21. Cell boundaries are clearly marked. (Sample No. 6).

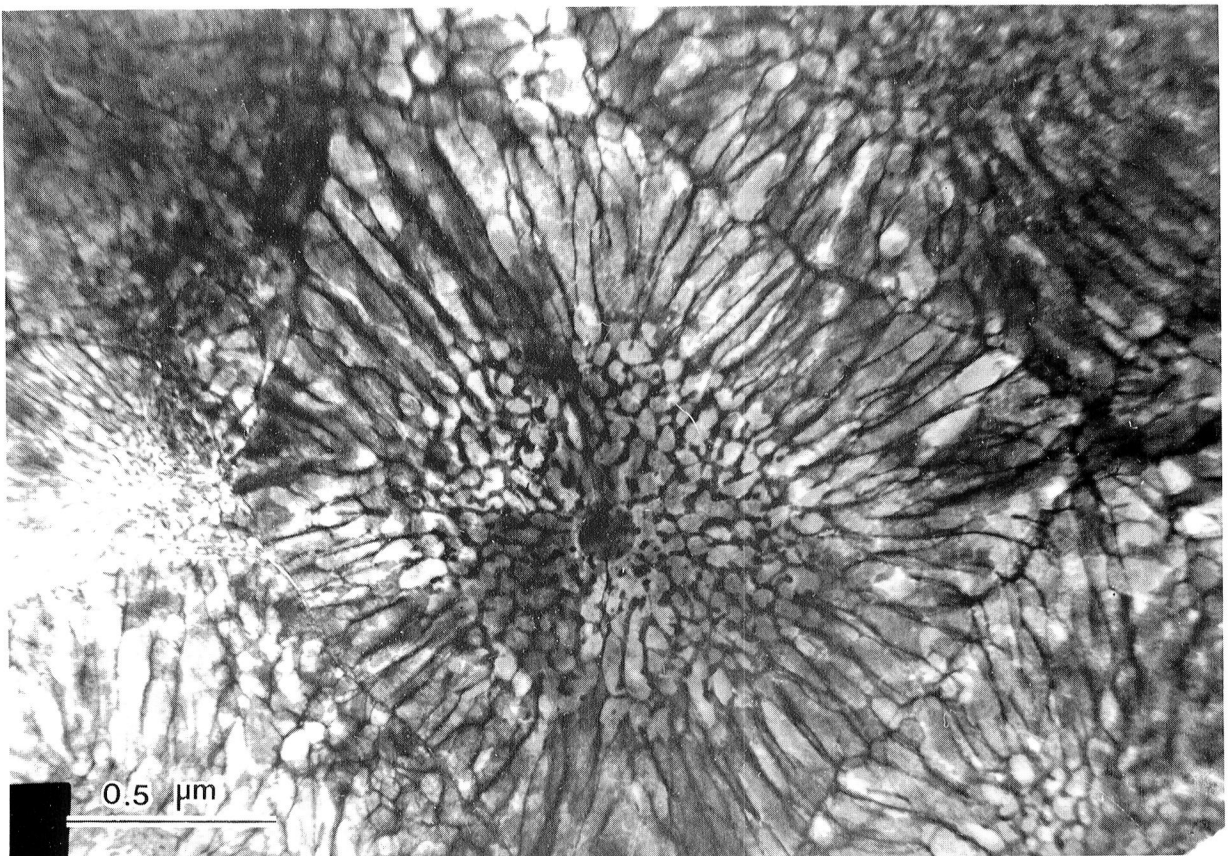


FIGURE 23.  
Al-4Cu-1Mg-1.5Fe-0.75Ce. Nucleation center at the interior of the particle. Such centers originate in a small spherulite that solidifies first. (Sample No. 6).



are seen emanating from it in all directions. This event is an example of one of many occurring in this location. It is not clear to us at this time what is the particle that serves as a nucleation site but previous experience indicates that such particles are rich in solute, and solidify first in the molten alloy. The cell sizes around the nucleation site indicate no large bulk undercooling, but rather a gradual extraction of heat to the environment.

c. Al-3 Li-1.5 Cu-1 Mg-0.5 Co-0.2 Zr (vacuum atomized, No. 2)

The microstructure of this alloy is also cellular with cell sizes reaching  $5\mu\text{m}$  (Fig. 24). This large cell size is to be expected in vacuum atomized powders where the heat is extracted from the solidifying particle by radiation only. The rates of heat extraction by radiation and by convection depend on the particle size. In the range of particle sizes examined in this study, convection is by far superior to radiation and results in a finer distribution of alloying elements within the particle. The lower solidification rate of the vacuum atomized particle results, also, in well defined particles segregated at the cell boundary as shown in the higher magnification Fig. 25.

d. Al-3 Li-1.5 Cu-1 Mg-0.5 Co-0.2 Zr (ultrasonic atomization in Ar, No. 3)

This powder exhibits a cellular microstructure (Fig. 26) with well defined cell boundaries and a high density of dislocations within the cells. The cell boundaries contain an almost continuous phase (Fig. 27) averaging  $0.1\mu\text{m}$  in thickness.



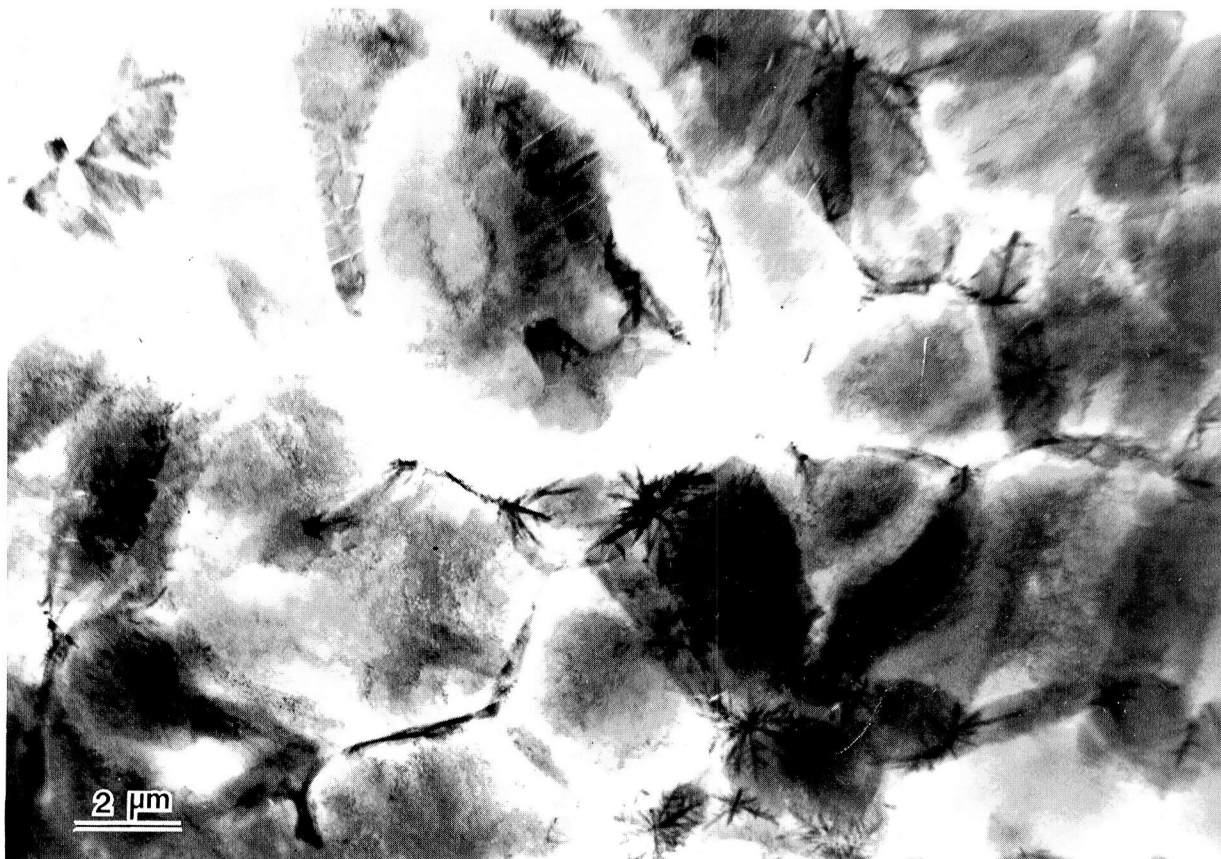


FIGURE 24.  
At-3Li-1.5Cu-1Mg-0.5Co-0.2Zr. Vacuum atomized. Large cells and feathery phase at the cell boundary. (Sample No. 2).

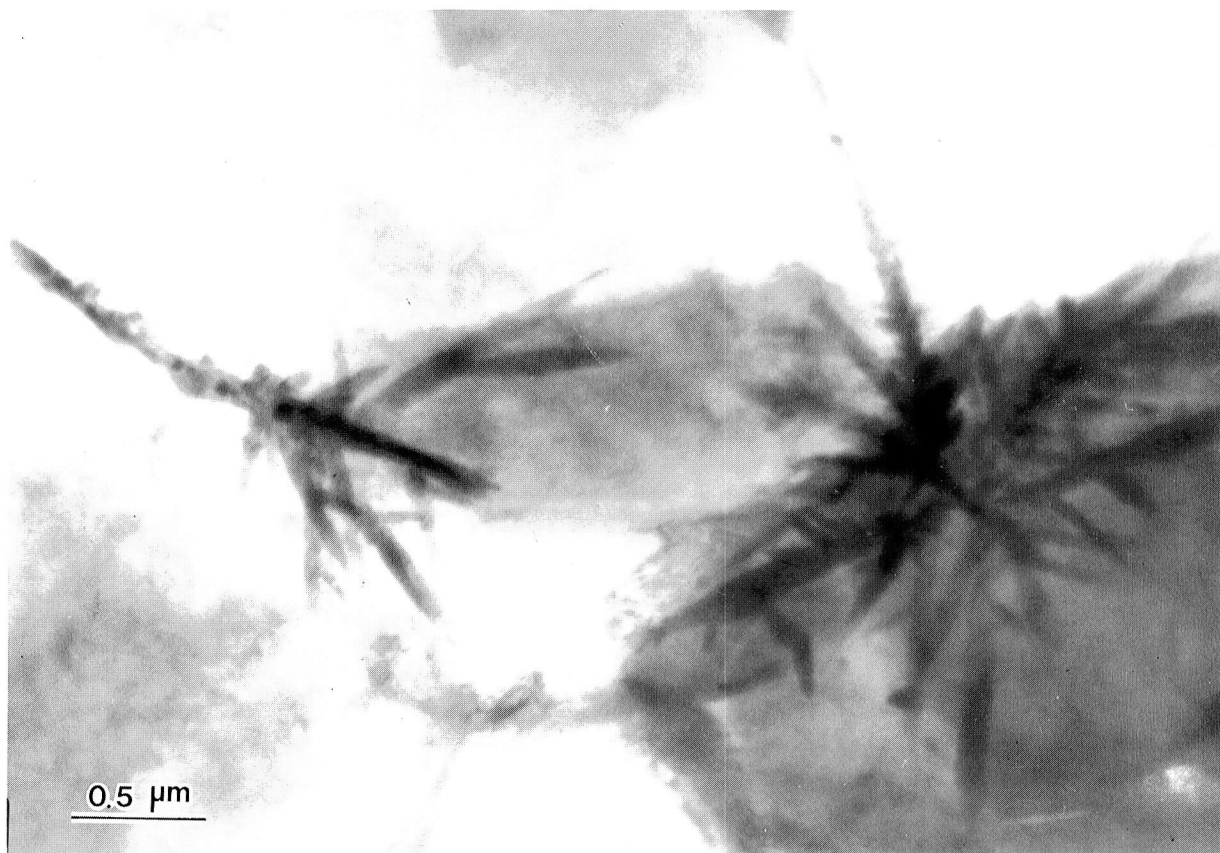


FIGURE 25.  
At-3Li-1.5Cu-1Mg-0.5Co-0.2Zr. Vacuum atomized. Feathery phase at all boundaries. (Sample No. 2).



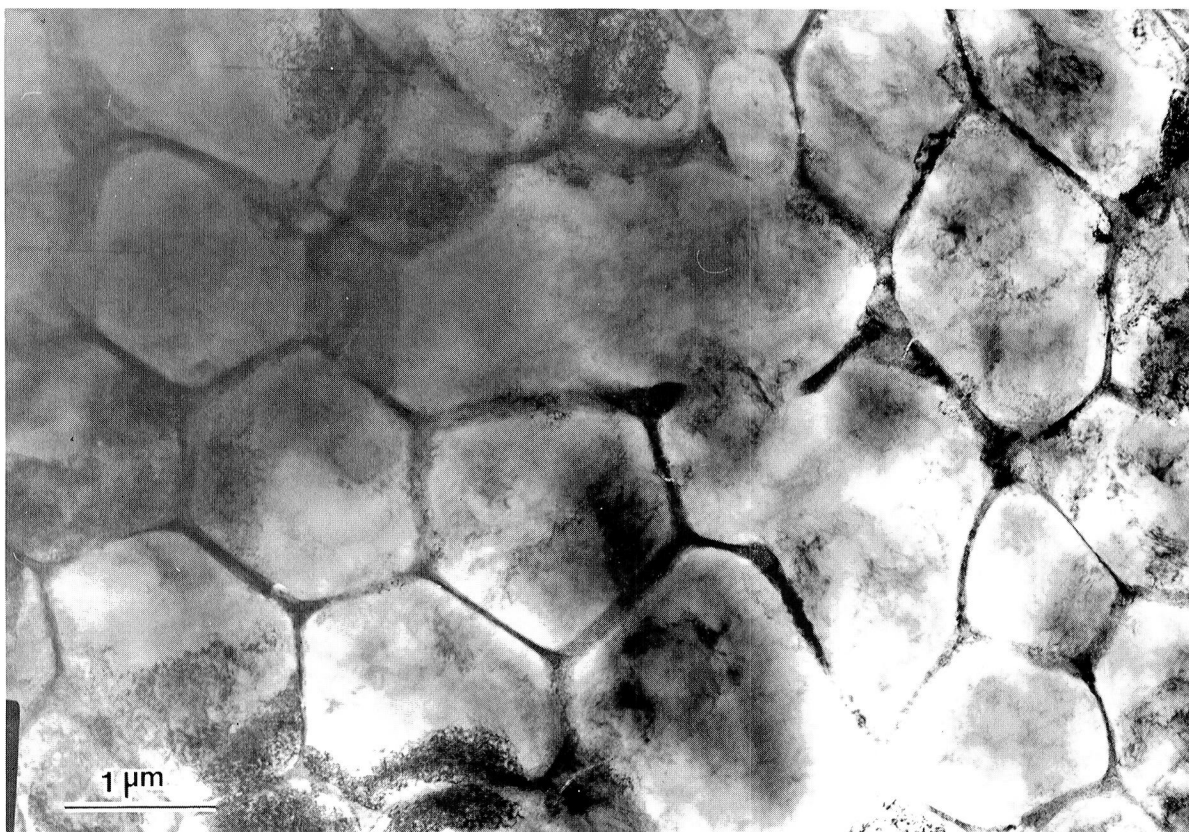


FIGURE 26.  
Al-3Li-1.5Cu-1Mg-0.5Co-0.2Zr. Ultrasonic atomization in argon. The cellular microstructure contains a phase at all the cell boundary and dislocations within the cells. (Sample No. 3).



FIGURE 27.  
Al-3Li-1.5Cu-1Mg-0.5Co-0.2Zr. Ultrasonic atomization in argon. A continuous phase at the cell boundary. (Sample No. 3).



The cell sizes are found to be up to  $2\mu\text{m}$  (i.e., finer than the vacuum atomized alloy #2 and similar to the helium atomized alloy #4). At certain locations within the grains the first stages of coherent precipitation are observed. This is demonstrated in Fig. 28 and in the selected area diffraction pattern shown in Fig. 29. Some of the precipitates reach 3nm in size but most of them are smaller. It is unlikely that this phenomenon is unique to the samples prepared by the atomization method. The phenomenon is rather isolated and does not represent the bulk of the powder.

- e. Al-3 Li-1.5 Cu-1 Mg-0.5 Co-0.2 Zr (ultrasonic atomization in He, No. 4)

Cellular microstructure is the type found in these particles too. Because of the relatively high rate of heat extraction all sizes are smaller than the ones found in the vacuum atomized powder, but reach the size of  $2\mu\text{m}$  (Fig. 30). The cell boundaries contain particles as shown in Fig. 31 and the cells contain a high density of dislocations (Fig. 32) indicating possible stress associated with first stage of precipitation. A certain proportion of the powder contains a high density of well defined particles (not identified at this stage). These particles can be seen in Fig. 33 and the diffraction pattern, which indicate coherency is presented in Fig. 34.

- f. Al-4.4 Cu-1.5 Mg-1 Fe-1 Ni-0.2 Zr (vacuum atomized, No. 5)

The microstructure of this alloy is also characterized by large cells that reach the size of  $5\mu\text{m}$  in length



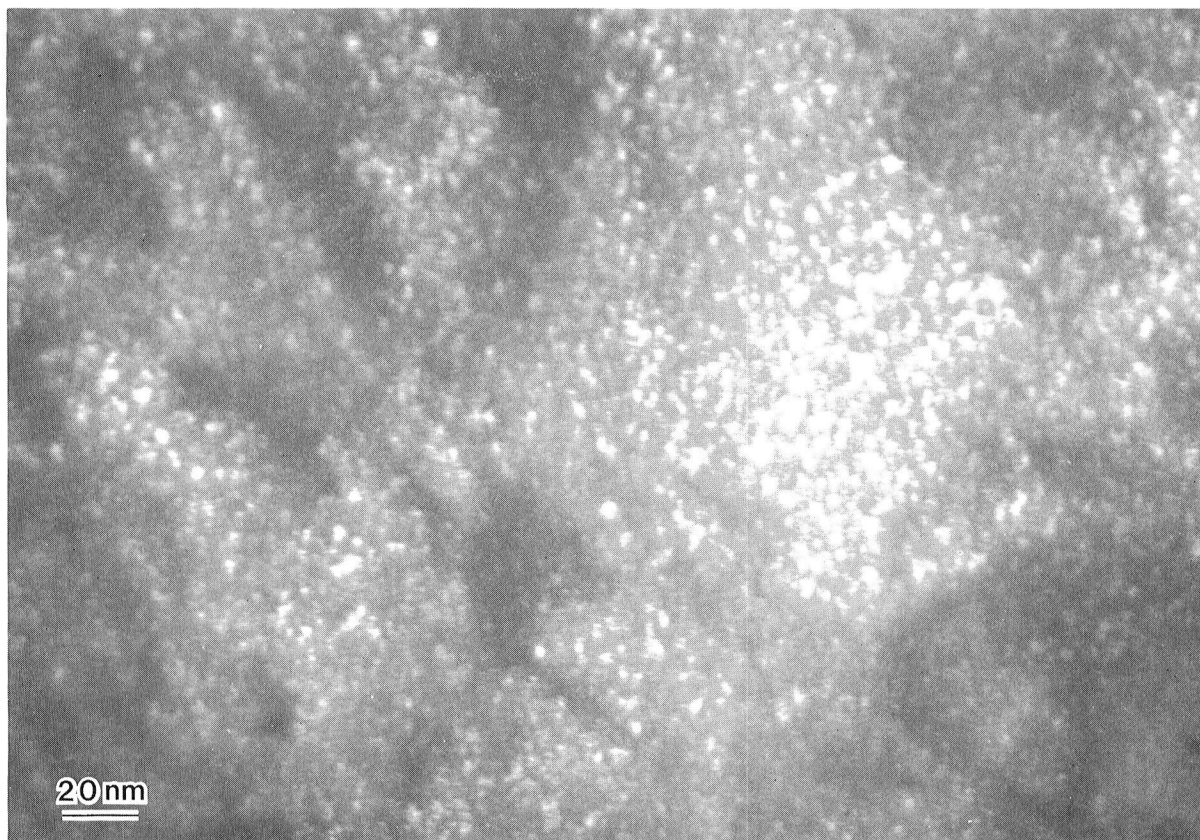


FIGURE 28.  
Al-3Li-1.5Cu-1Mg-0.5Co-0.2Zr. Ultrasonic atomization in argon. Fine precipitates within the cells. (Sample No. 3).

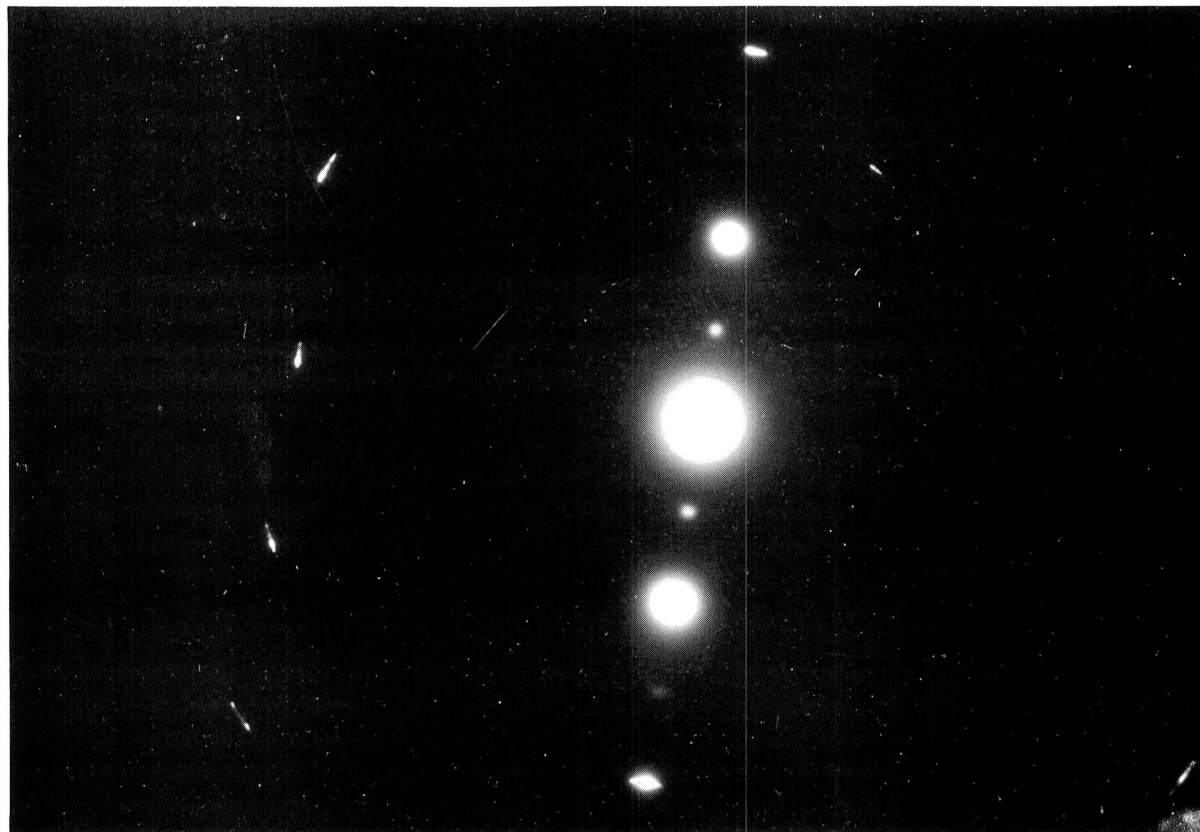


FIGURE 29.  
Al-3Li-1.5Cu-1Mg-0.5Co-0.2Zr. Ultrasonic atomization in argon. Selected area diffraction pattern indicates extra spots at half distance of the (002) reflection originated from fine particles in Figure 28. (Sample No. 3).



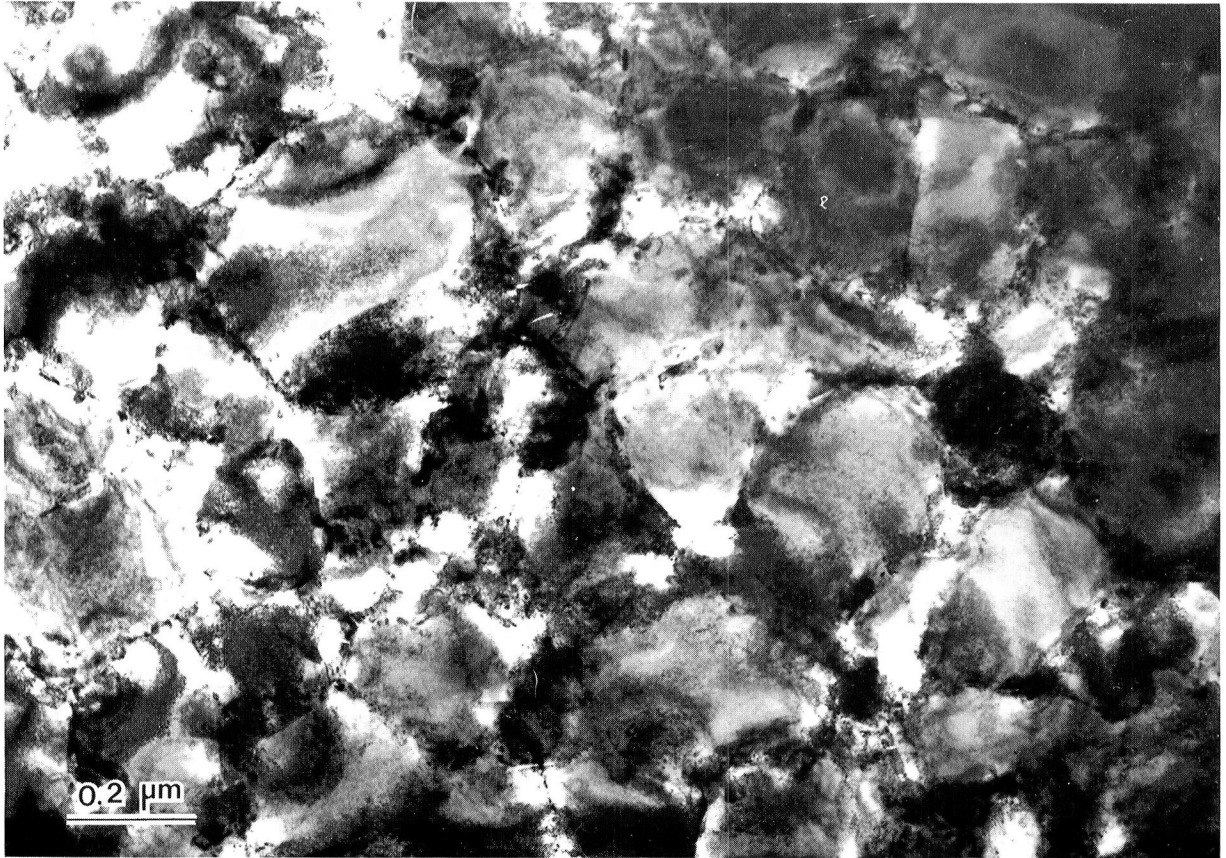


FIGURE 30.  
Al-3Li-1.5Cu-1Mg-0.5Co-0.2Zr. Ultrasonic atomization in helium. A cellular microstructure. Cell size is up to  $2\mu\text{m}$  and the cells are heavily strained. (Sample No. 4).

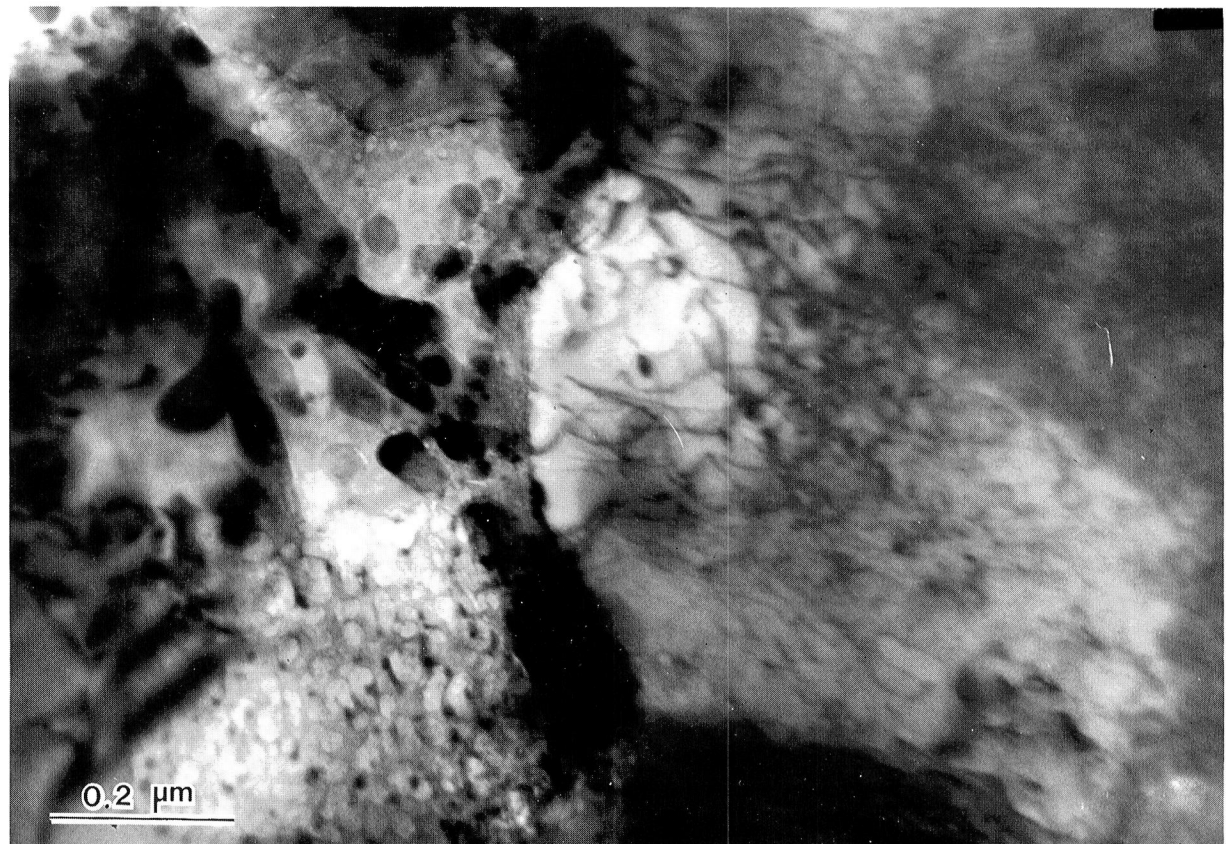


FIGURE 31.  
Al-3Li-1.5Cu-1Mg-0.5Co-0.2Zr. Ultrasonic atomization in helium. Particles at cell boundaries. (Sample No. 4).



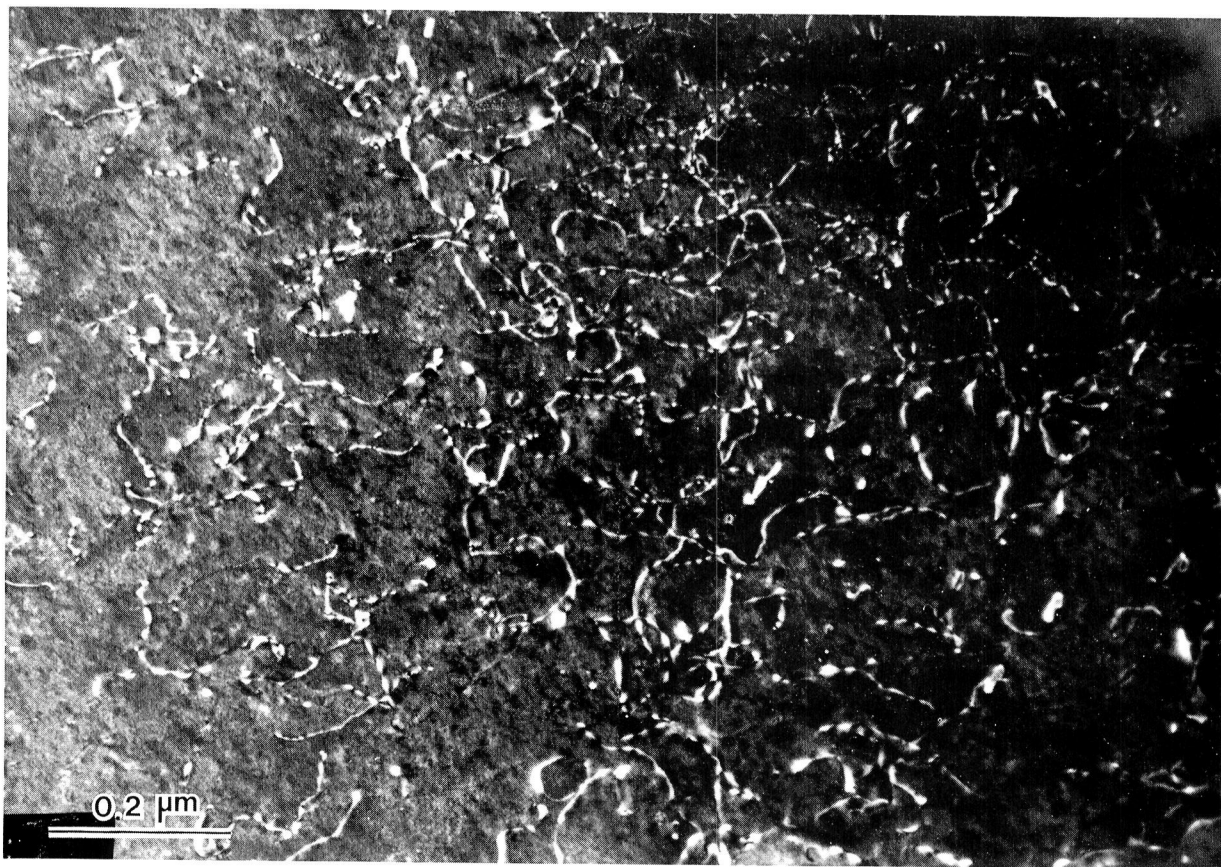


FIGURE 32.  
Al-3Li-1.5Cu-1Mg-0.5Co-0.2Zr. Ultrasonic atomization in helium. High density of dislocation within the cells, weak beam dark field. (Sample No. 4).

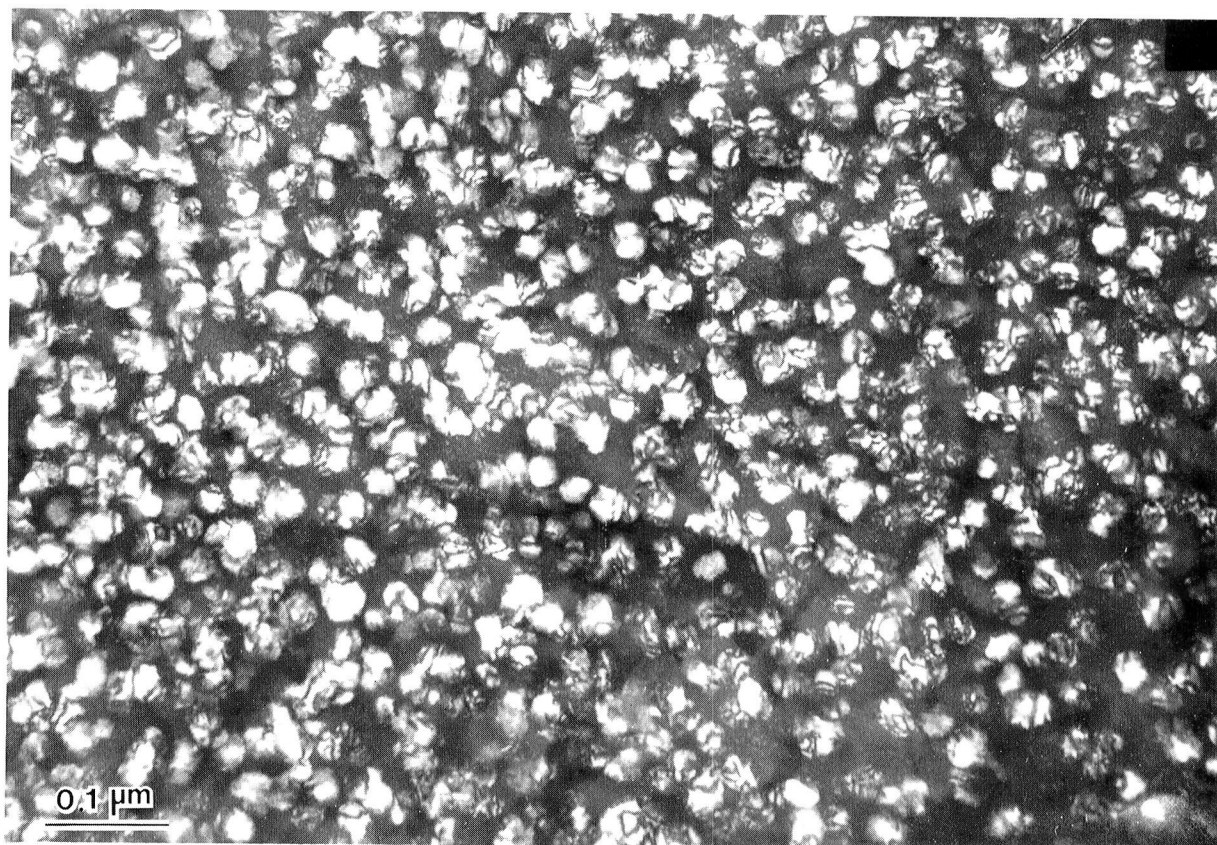


FIGURE 33.  
Al-3Li-1.5Cu-1Mg-0.5Co-0.2Zr. Ultrasonic atomization in helium. High density of particles in some of the cells. (Sample No. 4).



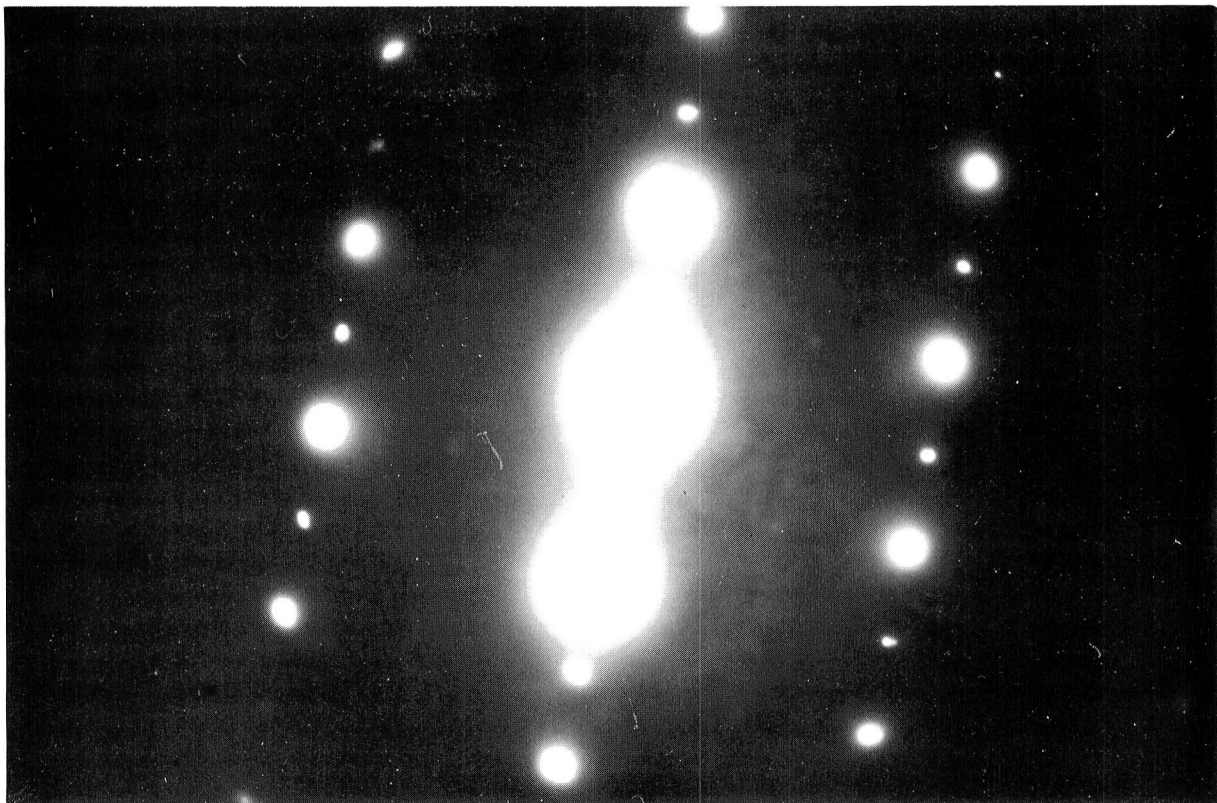


FIGURE 34.  
Al-3Li-1.5Cu-1Mg-0.5Co-0.2Zr. Ultrasonic atomization in helium. Selected area diffraction pattern of particles in Figure 33.  
(Sample No. 4).

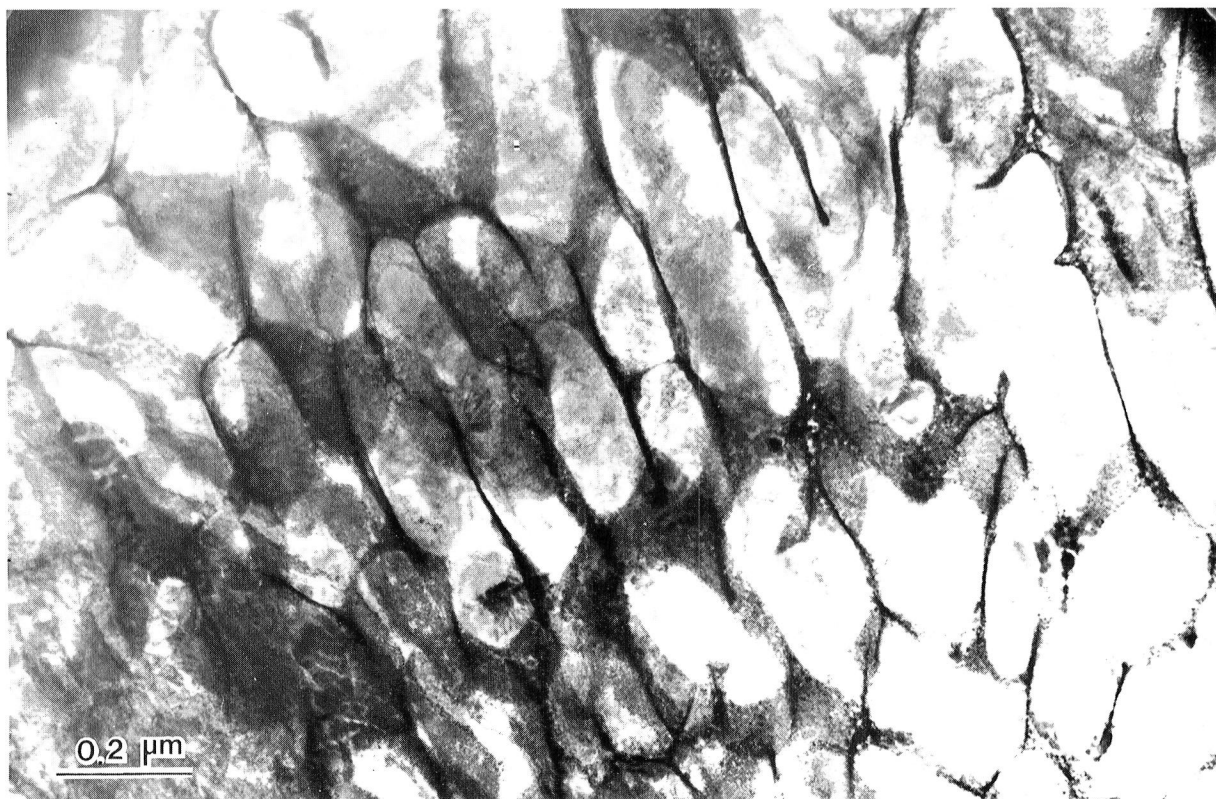


FIGURE 35.  
Al-4.4Cu-1.5Mg-1Fe-1Ni-0.2Zr. Vacuum atomized powder. Large cells, measuring up to 5 μm in length are formed. (Sample No. 5).



(Fig. 35). The cell boundary is decorated by small particles (Fig. 36). The cell interior contains a high density of dislocations as seen in Fig. 37 which is a weak beam dark field image using the (111) operating reflection.

#### 4. Elemental Distribution in the Cellular Structure

Compositional analysis in the cell and on the cell boundary was performed on two of the alloys; Al-4 Cu-1 Mg-1.5 Fe-0.75 Ce (Sample No. 6) and Al-4.4 Cu-1.5 Mg-1 Fe-1 Ni-0.2 Zr (Sample No. 5). The analysis was performed in the STEM using a convergent beam. Table A summarizes the results obtained from the first microstructure and Table B, the one obtained from Sample No. 5 alloy (Al-4.4 Cu-1.5 Mg-1 Fe-1 Ni-0.2 Zr). Each result in the tables represents five measurements, 200 seconds each. The fourth and fifth column give the relative intensities of each of the alloying elements to that of the aluminum in the point under study. The sixth column gives the ratio of the values of column four and five. The ratio in column six can be considered as a measure of the segregation ratio, or the tendency of alloying elements to concentrate at cell boundary.

This can be illustrated in the following formulation:

In a thin section --

$$\frac{C_{A1}}{C_{B1}} = k_{AB} \frac{I_{A1}}{I_{B1}}$$

where: C - concentration

Index A, B - elements A and B

Index 1 - indicates a point in the cell center

Index 2 - indicates a point in the cell boundary

I - x-ray intensity (number of counts per unit time)

$k_{AB}$  - proportionality coefficient



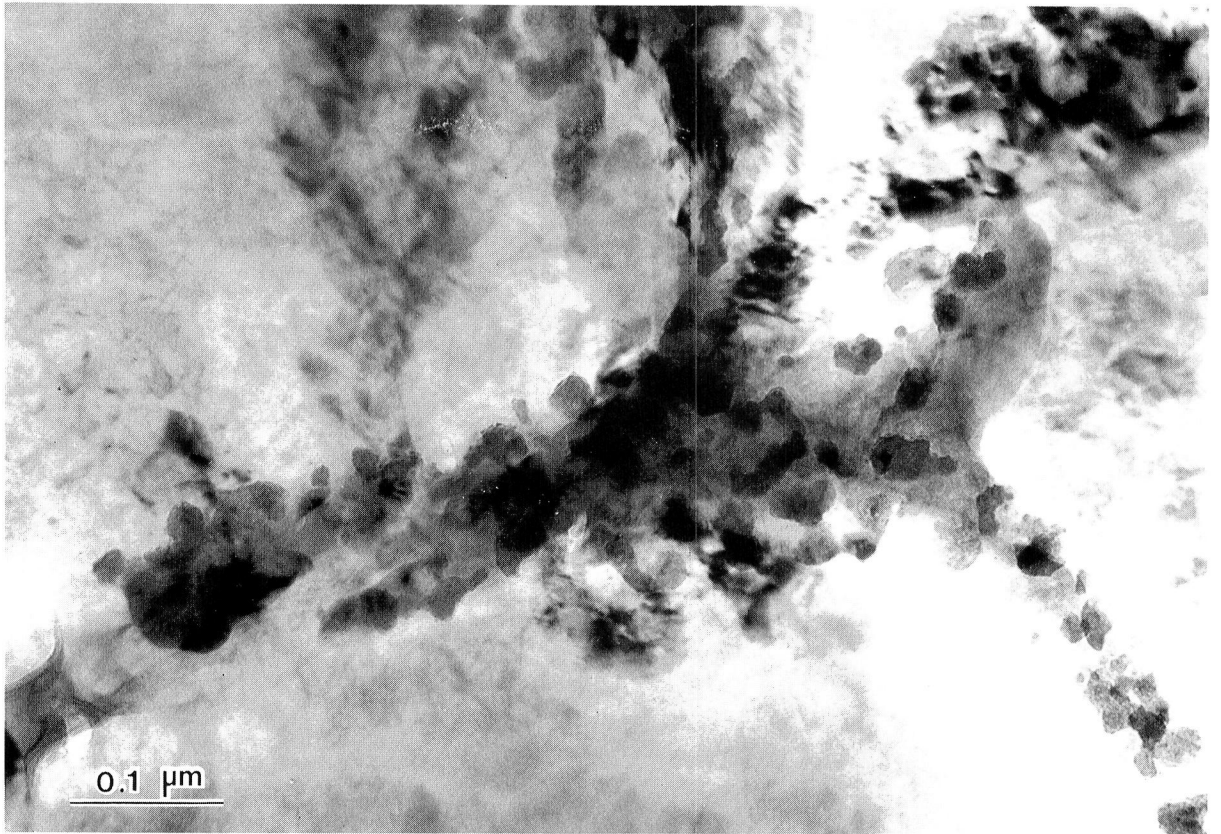


FIGURE 36.  
Al-4.4Cu-1.5Mg-1Fe-1Ni-0.2Zr. Vacuum atomized powder. Particles are formed at the cell boundary. (Sample No. 5).

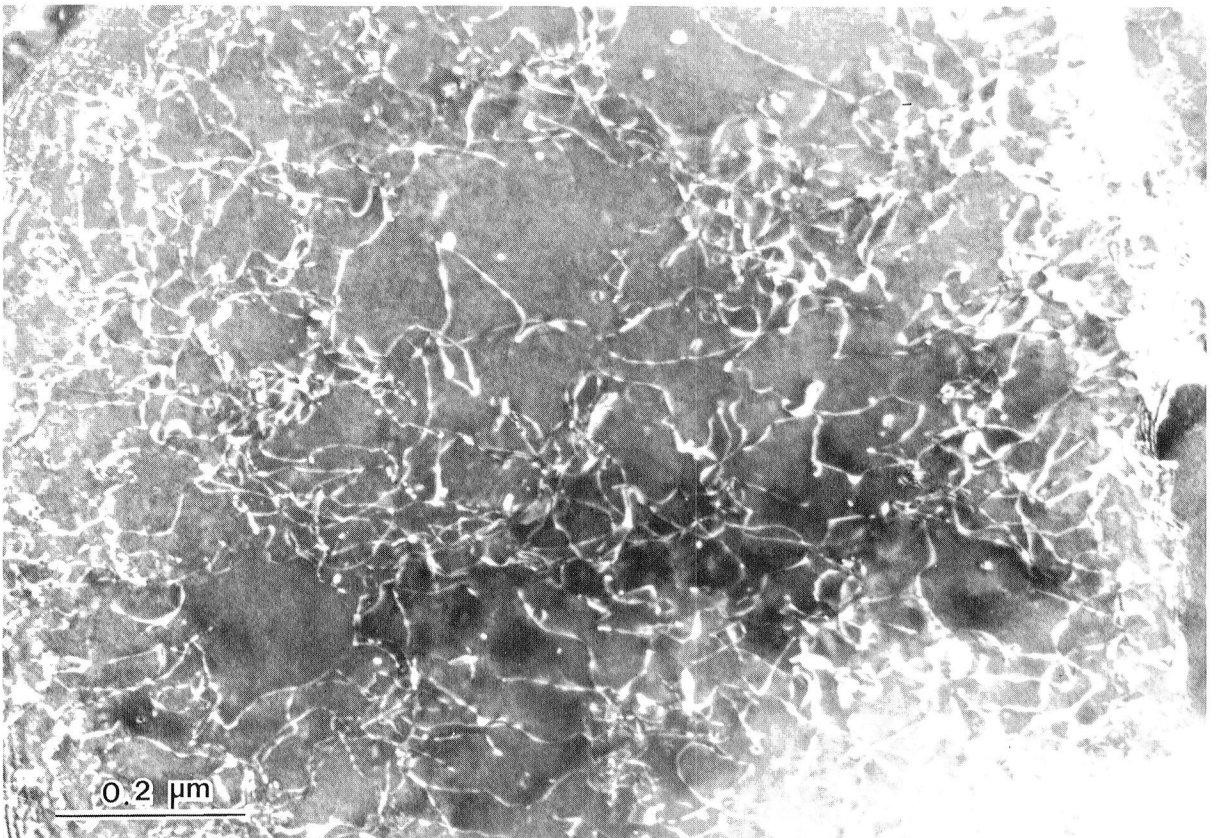


FIGURE 37.  
Al-4.4Cu-1.5Mg-1Fe-1Ni-0.2Zr. Vacuum atomized powder. The cell interior contains a high density of dislocations. (Sample No. 5).



in the cell center: 
$$\frac{C_{A1}}{C_{B1}} = k_{AB} \frac{I_{A1}}{I_{B1}}$$

in the cell boundary: 
$$\frac{C_{A2}}{C_{B1}} = k_{AB} \frac{I_{A2}}{I_{B2}}$$

dividing the equations: 
$$\frac{\frac{C_{A1}}{C_{B1}}}{\frac{C_{A2}}{C_{B1}}} = \frac{\frac{I_{A1}}{I_{B1}}}{\frac{I_{A2}}{I_{B2}}}$$

Example: The ratio of Fe in the alloy Al-4 Cu-1 Mg-1.5 Fe-0.75 Ce

$$\frac{\frac{C_{Fe_2}}{C_{Al_2}}}{\frac{C_{Fe_1}}{X_{Al_1}}} = \frac{\frac{2851}{10298}}{\frac{80}{23105}} = 79.9$$

This value indicates a high tendency for segregation of the iron in the cell boundary. The ratio for copper is 9.27 indicating a lower tendency for segregation and that of magnesium is 2.13, indicating an even lower tendency.

Element	$I_2$ counts in cell boundary	$I_1$ counts in cell	$\frac{I_{2x}}{I_{2Al}} \times 100$	$\frac{I_{1x}}{I_{1Al}} \times 100$	$\frac{C_{2x}}{C_{2Al}} \frac{C_{1x}}{C_{1Al}}$
Al	10298	23105			
Mg	209	220	2.03	0.95	2.13
Ce	125	75	1.21	0.32	3.74
Fe	2851	80	27.7	0.35	79.9
Cu	2557	619	24.8	2.68	9.27

TABLE A: Compositional analysis of cell interior and cell boundary for the alloy Al-4 Cu-1 Mg-1.5 Fe-0.75 Ce (Sample No. 6) (see text).

Element	$I_2$ counts in cell boundary	$I_1$ counts in cell	$\frac{I_{2x}}{I_{1Al}}$ x100	$\frac{I_{1x}}{I_{1Al}}$ x100	$\frac{C_{2x}}{C_{2Al}} \cdot \frac{C_{1x}}{C_{1Al}}$
Al	12847	27511			
Mg	544	650	4.23	2.36	1.79
Fe	2684	180	20.9	0.65	31.9
Ni	2135	420	16.6	1.53	10.9
Cu	5499	2579	42.8	9.37	4.6
Zr	50	210	0.39	0.76	0.5

TABLE B: Compositional analysis of cell interior and cell boundary for the alloy Al-4.4 Cu-1.5 Mg-1 Fe-1 Ni-0.2 Zr (Sample No. 5).

The equilibrium partition coefficients for the solidification of the binary alloys that contain, as an alloying element, the elements present in the alloy under study, give a good indication of which element tends to segregate more in the cell boundary. The smaller the partition coefficient the larger is the tendency to segregate. Table C lists the various partition coefficients, and it correlates with the experimental results in Tables A and B. Note that the Zr is different than the other elements in that its binary diagram is peritectic and not eutectic like the others. The partition coefficient is larger than one, and thus this element tends to segregate away from the cell boundary (see also result in Table B).

Al-Mg	- 0.42
Al-Fe	- 0.03
Al-Ni	- 0.008
Al-Cu	- 0.17
Al-Ce	- 0.003
Al-Li	- 0.4
Al-Zr	- 2.5

TABLE C: Equilibrium partition coefficients for solidification of primary aluminum phase.

### SUMMARY

Microstructural features of seven aluminum base alloy powder were studied by optical metallography, scanning electron microscopy and transmission electron microscopy. The alloys exhibit a cellular structure with characteristics which vary with the composition of the alloys and the solidification procedure employed. Examples of the various microstructural features and a discussion about their formation is presented. One of the alloys, Al-3Li-1.5Cu-1Mg-0.5Co-0.2Zr (roller quenched flakes) was not evaluated by the transmission electron microscope. This alloy is being studied now and will be reported on in the next report. This progress report will also summarize the study of the effect of heat treatments on the development of the microstructure of the alloys.





